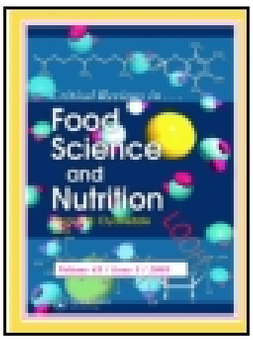

Critical Reviews in Food Science and Nutrition

ISSN: (Print) (Online) Journal homepage: https://www.tandfonline.com/loi/bfsn20

# Recent developments in vibrational spectral analyses for dynamically assessing and monitoring food dehydration processes

Yuqiao Ren, Xiaohui Lin, Tong Lei & Da-Wen Sun

**To cite this article:** Yuqiao Ren, Xiaohui Lin, Tong Lei & Da-Wen Sun (2021): Recent developments in vibrational spectral analyses for dynamically assessing and monitoring food dehydration processes, Critical Reviews in Food Science and Nutrition, DOI: 10.1080/10408398.2021.1947773

**To link to this article:** https://doi.org/10.1080/10408398.2021.1947773

Published online: 19 Jul 2021.

CRITICAL REVIEWS IN FOOD SCIENCE AND NUTRITION
https://doi.org/10.1080/10408398.2021.1947773

Taylor & Francis
Taylor & Francis Group

REVIEW



# Recent developments in vibrational spectral analyses for dynamically assessing and monitoring food dehydration processes

Yuqiao Ren, Xiaohui Lin, Tong Lei, and Da-Wen Sun

Food Refrigeration and Computerized Food Technology (FRCFT), School of Biosystems and Food Engineering, Agriculture & Food Science Centre, University College Dublin (UCD), National University of Ireland, Belfield, Dublin 4, Ireland

**ABSTRACT**

Dehydration is one of the most widely used food processing techniques, which is sophisticated in nature. Rapid and accurate prediction of dehydration performance and its effects on product quality is still a difficult task. Traditional analytical methods for evaluating food dehydration processes are laborious, time-consuming and destructive, and they are not suitable for online applications. On the other hand, vibrational spectral techniques coupled with chemometrics have emerged as a rapid and noninvasive tool with excellent potential for online evaluation and control of the dehydration process to improve final dried food quality. In the current review, the fundamental of food dehydration and five types of vibrational spectral techniques, and spectral data processing methods are introduced. Critical overtones bands related to dehydration attributes in the near-infrared (NIR) region and the state-of-the-art applications of vibrational spectral analyses in evaluating food quality attributes as affected by dehydration processes are summarized. Research investigations since 2010 on using vibrational spectral technologies combined with chemometrics to continuously monitor food quality attributes during dehydration processes are also covered in this review.

**KEYWORDS**

Vibrational spectral technology; dehydration; chemometrics; physical attributes; chemical components

## Introduction

As one of the most important processes, dehydration or drying is widely used in the food industry. With the global trades requiring long-life products and the pursuit of consumers for high-quality food, various dehydration techniques have been developed for the food industry (Liu, Pu, and Sun 2017). During dehydration, heat and mass transfer occur simultaneously, which reduces the moisture content of the food to the required level and prevent the growth of moisture-related microorganisms from spoiling perishable food. Therefore, dehydration can not only extend the shelf life but also reduce the mass and volume of food, thus improving the stability of foods and cost-effectiveness of packaging, transportation and storage.

Currently, many dehydration techniques are available in the food industry. Air drying, microwave drying, freeze-drying, and solar drying are the most commonly used methods for food dehydration (Li et al. 2020), while other techniques, such as heated-dehydration (H-D), brined-dehydration (B-D), infrared drying, microwave vacuum drying (MVD), vacuum freezing drying (VFD), contact ultrasound-assisted hot air drying (CUHAD), microwave-assisted pulse-spouted bed vacuum-drying (PSMVD), pulse-spouted microwave freeze-drying (PSMFD), have also been developed for enhancing dehydration performance. For obtaining high quality dehydrated products, dynamic evaluation and control of the dehydration process are important. Because during the dehydration process, the change of food quality attributes, such as moisture content, sensorial attributes and chemical components, are directly related to dehydration conditions such as temperature, airflow rates, air pressure, etc. Modifying dehydration conditions based on dynamic product quality evaluation enables the maintaining of the quality of dehydrated products to the required level (Stawczyk et al. 2009; Amjad et al. 2018; Li et al. 2020).

Traditional methods in evaluating and controlling dehydration processes mainly rely on destructive, laborious, cumbersome and time-consuming strategies, containing thermo-gravimetric method and Karl Fisher titration for moisture content analyses, colourimeter analysis for chromaticity evaluation, texture profile analysis, Warner-Bratzler shear test, and Magness-Taylor penetration test for texture analysis, and analytical chemistry testing along with sample pre-processing for chemical components evaluation, making these methods not suitable for on-line monitoring (Ma et al. 2017; Qu et al. 2017; Sturm et al. 2020).

On the other hand, vibrational spectral technologies, as an integrating term referring to spectral imaging techniques (Wu and Sun 2013a, 2013b) and spectroscopic techniques of near-infrared (NIR) (Porep, Kammerer, and Carle 2015), mid-infrared (MIR) (Su and Sun 2018), Terahertz (THz) (Wang, Sun, and Pu 2017), and Raman (Yaseen, Sun, and Cheng 2017), have emerged as a series of rapid, noninvasive and accurate analysis techniques, which can not only significantly minimize time-consuming laborious work and

CONTACT Da-Wen Sun dawen.sun@ucd.ie http://www.ucd.ie/refrig, http://www.ucd.ie/sun

provide valuable information relevant to physicochemical parameters of dehydrated samples, but can also be easily integrated into existing drying systems to evaluate or even control dehydration processes (Collell et al. 2012; Stawczyk et al. 2009). Therefore, many studies have been performed and significant developments have been made in using vibrational spectral analyses for evaluating and controlling food dehydration processes in recent years.

Several reviews have been published on nondestructive measurement tools to analyze food drying processes. Li and Qian (2017) compared different imaging techniques used in the drying field, namely scanning electron microscopy (SEM), neutron radiography (NR), magnetic resonance imaging (MRI), charge-coupled device (CCD) photography and X-ray tomography. Liu, Pu, and Sun (2017) discussed the strengths and weaknesses of hyperspectral imaging (HSI) to monitor different food processes, including hot-air, microwave, and freeze-drying processes, for products quality and safety assurance. Li et al. (2020) reviewed the application of nondestructive techniques such as electronic nose (E-nose), computer vision (CV), HSI, near-infrared spectroscopy (NIRS), nuclear magnetic resonance (NMR) and dielectric spectroscopy for sensing multiple attributes of food quality undergoing the air, freezing, solar and microwave drying. Despite these reviews, no review on vibrational spectral techniques for the evaluation and monitoring of food dehydration processes has been published, and no summary of different vibrational spectral analyses for monitoring critical attributes in food dehydration processes is available yet. Therefore, the current review aims to discuss, compare and summarize the application of vibrational spectral analysis techniques, including NIRS, mid-infrared spectroscopy (MIRS), terahertz time-domain spectroscopy (THz-TDS), Raman spectroscopy, and spectral imaging, coupled with chemometric methods for dynamically evaluating and controlling food dehydration processes.

## Fundamentals

### Dehydration processes

Dehydration processes aim to reduce samples moisture content (MC) to a required level, which generally lower MC to less than 10% or water activity ($a_w$) to about 0.60-0.65 (Zambrano et al. 2019). A high-quality dehydration process should rapidly, uniformly, and energy-efficiently remove MC from samples with minimal damage to heat-sensitive components and microstructure. Nevertheless, mass and heat transfer simultaneously happen during food thermal dehydration, leading to intensive biochemical reactions and physical changes (Cui et al., 2004a; Cui et al., 2004b; Cui et al., 2005). Therefore, food dehydration is sophisticated, non-linear, and hard-foreseeable, which is imperfectly understood yet. Although osmatic dehydration and mechanical dewatering are commonly used in the food industry, most dehydration methods are based on thermal dewatering (Zhang et al. 2017). Convective drying, microwave drying, freeze-drying, and solar drying are the four most popular methods in the food industry (Li et al. 2020). However, due to the low thermal conductivity of foods, convective drying requires lengthy drying time with low energy-efficiency of around 35-45% on average and in some cases even lower than 10% (Crichton et al. 2018). Solar drying is a low-cost technique with low energy consumption, but the prolonged exposure to solar radiation and hot air bring undesirable nutrition loss and physicochemical change to samples (Cheng et al. 2019; Tunde-Akintunde 2011). Microwave drying is convenient and energy-efficient with relatively short processing time, widely applied in both the food industry and domestic households, but the non-uniform temperature distribution and over-heating of certain spots exist in the product (Chandrasekaran, Ramanathan, and Basak 2013; Guo et al. 2017; Cui et al., 2003). Freeze drying is considered the technique producing the best dehydrated products, but to maintain extremely low pressure and temperature, its energy consumption could be four to ten times higher compared with hot air drying (Bhatta, Stevanovic Janezic, and Ratti 2020). Therefore, developing rapid, reliable, and nondestructive spectral analyses to dynamically assessing and monitoring dehydration processes is important for process optimization and product quality enhancement (Gonzalez-Mohino et al. 2020; Ma et al. 2017).

### Vibrational spectral techniques

Spectral techniques analyze the interaction between different electromagnetic radiation and target matter (Dufour 2009; Sathyanarayana 2004). Continuous vibration within molecule systems results in permanent oscillate change and induces dipole moments, where the former can be analyzed by infrared (IR) spectral techniques and Raman spectral technique is able to assess the latter, while THz waves, located at the conjunction of infrared and submillimeter regions, show great potential to evaluate food dehydration (Afsah-Hejri et al. 2019).

### Infrared spectral techniques

Infrared radiation covers the wavelength range between about 780 and 300,000 nm on the electromagnetic spectrum, which can be divided into NIR (780-2500 nm), MIR (2500-25,000 nm) and far-infrared (25,000-300,000 nm) (Su, Bakalis, and Sun 2018). There is a limited application of far-infrared spectral analyses within food science because of the low absorbance of most molecules in this region, except typical heavy molecules (Smith 2003; Craig, Franca, and Irudayaraj 2015). MIR bands assign each absorption peak to a specific molecule, while the NIR region covers overlapping absorptions corresponding to both overtones and combined vibrational modes of C-H, N-H, and O-H, indicating the existence of carbohydrates or fat, protein or amine, and MC, respectively (Huang et al. 2008; Lei and Sun 2019; Nunes 2014; Pedreschi, Segtnan, and Knutsen 2010). Table 1 summarizes the typical overtones of these bonds in the NIR region, and the MIR and NIR spectra of water are exhibited in Figure 1 as an example. Water molecules exhibit strong absorbance in the spectrum, where the intense absorbance exists at 3300 and 1638 $cm^{-1}$ in the MIR region and 1442 and 1932 nm in the NIR region (Dufour 2009). Several studies indicate that NIR based chemometric models show better MC prediction ability than models based on MIR (Ferreira et al. 2014; Shi and Yu 2017; Su, Bakalis, and Sun 2019b). Besides, the spectral range of visible-near-infrared (VNIR), as the

**Table 1.** Summary of critical overtones of NIR region in dehydration processes evaluation.

| Interpretation | Wavelengths (nm) | Reference |
|---|---|---|
| O-H stretching 1st overtone | 1190-1941 | Su and Sun (2017), Su, Bakalis, and Sun (2019b), Lin, Xu, and Sun (2020b), Netto et al. (2021), Collell et al. (2011) |
| O-H stretching 2nd overtone | 960-977 | Sun et al. (2020), Pu et al. (2018), Lee et al. (2020), Su, Bakalis, and Sun (2019b) |
| O-H stretching 3rd overtone | 730-1000 | Liu, Sun, and Zeng (2014), Xu, Gowen, and Sun (2018), Ma, Sun, and Pu (2017), Liu et al. (2018), Wu, Shi, et al. (2012) |
| C-H stretching 1st overtone | 1706-1761 | Pu and Sun (2015), Chakravartula et al. (2019), Collell et al. (2012) |
| C-H stretching 2nd overtone | 1153-1250 | Pu and Sun (2015), Su and Sun (2017), Wu, Wang, et al. (2012), Collell et al. (2011) |
| C-H stretching 3rd overtone | 840-934 | Sun et al. (2017), Wu, Shi, et al. (2012), Liu, Sun, and Zeng (2014) |
| C-H stretching 4th overtone | 760-762 | Sturm et al. (2020), Liu, Sun, and Zeng (2014) |
| N-H stretching 1st overtone | 1500-1570 | Wu, Wang, et al. (2012), Chakravartula et al. (2019), Achata et al. (2021) |
| N-H stretching 2nd overtone | 1040 | Liu, Sun, and Zeng (2014) |
| N-H stretching 3rd overtone | 775-880 | Sun et al. (2017), Yang, Sun, and Cheng (2017), Wu, Shi, et al. (2012) |

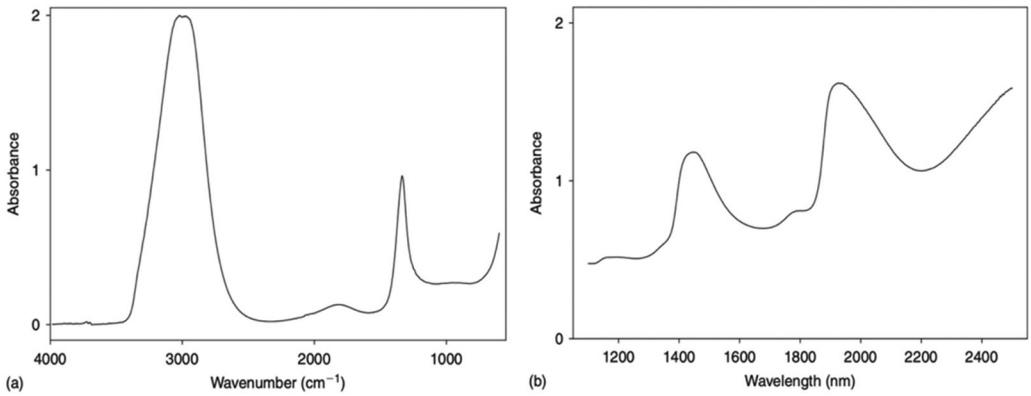


**Figure 1.** (a) Water mid-infrared and (b) near-infrared spectra (Dufour 2009).

combination of visible and short-wave infrared (SWIR) region, is commonly adopted in relevant research (Table 2).

The development of IR spectral instruments promotes research and applications of food dehydration assessment. Fourier-transform infrared spectroscopy (FTIR) normally refers to MIRS, as almost all the MIRS are based on interferometers instead of dispersive spectrometers (Craig, Franca, and Irudayaraj 2015). Besides, an extensive range of NIRS devices has been adopted in dehydration evaluation, such as Fourier-transform near-infrared spectroscopy (FT-NIRS) (Sinelli et al. 2011), dispersive NIR spectrometer (Kauppinen et al. 2013), acoustic-optical tunable filter spectrometer (Moscetti, Raponi, et al. 2018), and hand-held portable devices (Gonzalez-Mohino et al. 2020). Among them, the cost-effective portable NIRS shows great potential for dehydration assessment (Collell et al. 2012; Gonzalez-Mohino et al. 2020; Moscetti, Raponi, et al. 2018; Wokadala et al. 2020). FT-NIRS with high scanning speed is available for spectral imaging, and sensor-based NIRS with optical fiber can be easily integrated with existing dehydration systems for remote sensing (Kauppinen et al. 2013).

### *Raman spectral techniques*

When samples illuminated by visible or infrared narrowband laser light, sample molecules are brought to a high-energy collision but momentary status. After that, both Rayleigh and Stokes scatterings happen. Most excited molecules relax back to their original energy status by releasing photons at the same wavelength as the laser light source (Rayleigh scattering), while a small part of excited molecules retain a proportion of energy and relax to the vibrationally excited states with a lower frequency exciting light (Stokes scattering). Raman spectral analyses are based on measuring Raman shifts, which are the energy difference between incident laser light and photons emitted by stokes scattering (Yaseen, Sun, and Cheng 2017). However, the weak signal intensity, fluorescence interferences and expensive sophisticated instruments are the main limitations for the applications of the technique. Several Raman devices, such as Fourier-transform Raman spectroscopy (FT-Raman), surface-enhanced Raman spectroscopy (SERS), and micro-Raman spectroscopy, have been developed to eliminate these drawbacks by improving the light source wavelength to relieve the fluorescence background, employing surface-enhanced techniques to enhance the signal intensity, and applying a light source in the visible region to improve the signal to noise ratio, quantum efficiency and allow spatial analyses (Braeuer et al. 2017; Craig, Franca, and Irudayaraj 2013; Delwiche 2015; Yaseen, Sun, and Cheng 2017). Although both Raman and IR spectral analyses are based on detecting molecule vibration, they complement each other in applications. Raman spectral technique is good at detecting the electrical polarizability changes, while IR spectral techniques are mainly used to measure the electrical dipole moment changes, making it sensitive to MC (Craig, Franca, and Irudayaraj 2013; Zheng and He 2014).

### *Terahertz spectral techniques*

THz-TDS is a novel spectral technology using frequencies from 0.1 to 10 THz, which integrates the impressive penetration of submillimeter waves and the fingerprint feature of IR spectral techniques. However, compared with other

**TABLE 2.** Applications of vibrational spectral techniques in evaluating dehydration processes.

| Samples | Quality indicators | Dehydration methods | Conditions | Spectral ranges | Critical wavelengths | Spectral techniques | Monitor schedules | Models | Best Results | References |
|---|---|---|---|---|---|---|---|---|---|---|
| Moisture Evaluation | | | | | | | | | | |
| Apple slices | MC | AD | Temp.: 50, 70 °C | 400-1010 nm | 540, 817, 977 nm | VNIR-HSI | 0, 30, 60, 90, 120, 150, 180, 240 300 min | PLSR | $R^2_p$ = 0.99 RMSEP = 1.56% | Crichton et al. (2018) |
| Apple disks | MC | AD | Temp.: 70 °C | 400-780 nm | 425, 426, 427, 428, 429, 445, 467, 496, 557, 583, 616, 646, 647, 648, 649, 650, 661, 690, 719, 728 nm | Vis-HSI | 1, 2, 3, 4, 5, 6 h | PLSR | $R^2_p$ = 0.9732 RMSEP = 5.1603 | Crichton, Sturm, and Hurlbert (2015) |
| Banana slices | MC | AD | Temp.: 90 °C | 400-1000 nm | – | cross-polarized VNIR-HSI | 0, 30, 60, 90, 120, 150, 180, 210 min | PLSR | $R^2_p$ = 0.97 RMSEP = 0.05 kg/kg | Nguyen-Do-Trong, Dusabumuremyi, and Saeys (2018) |
| Banana slices | MC | MVD | Power: 250 W Pressure: 2000 Pa | 950-1650 nm | – | NIR-HSI | 3, 6, 9, 10, 12, 14, 15, 18, 19, 21 min | SVMR | $R^2_p$ = 0.996 RMSEP = 1.575% | Pu et al. (2018) |
| Beef jerky | MC | HAD | Temp.: 60 °C | 880-1720 nm | 27 selected bands | NIR-HSI | 30, 60, 90, 120, 150, 180, 210, 240 min | EMCVS | $R^2_p$ = 0.98 RMSEP = 0.14 RPD = 6.5 | Achata et al. (2021) |
| Beef slices | MC | AD | Temp.: 70 °C | 400-1010 nm | 571, 582, 583, 912, 948 nm | VNIR-HSI | 1, 2, 3, 4, 5, 6 h | CARS-PLSR | $R^2_p$ = 0.97 RMSEP = 0.08 | von Gersdorff et al. (2018) |
| Beef slices | MC | AD | Temp.: 68 °C | 400-1010 nm | 822, 961, 971, 974, 1005 nm | VNIR-HSI | 1, 2, 3, 4, 5, 6 h | MCUVE-PLSR | $R^2_p$ = 0.98 RMSEP = 0.12 | Retz et al. (2017) |
| Beef slices | MC | MD | Power: 500 W | 400-1000 nm | 427, 457, 523, 587, 605, 624, 670, 875, 959 nm | VNIR-HSI | 0, 30, 45, 60, 75 s | SPA-LS-SVM | $R^2_p$ = 0.869 RMSEP = 1.304 RPD = 2.724 | Liu et al. (2018) |
| Beef slices | MC | AD | Temp.: 40 °C | 380-1030 nm 900-1700 nm | 518, 669, 761, 874, 989, 1030 nm | VNIR-HSI | 0, 30, 60, 120, 180, 240 min | PCA SPA-MLR | $R^2_v$ = 0.969 RMSECV = 1.044% | Wu, Wang, et al. (2012) |
| Beef slices | MC | HAD | Temp.: 50, 60, 70 °C Air velocity: 0.6 m/s | 500-1009 nm | 500, 518, 543, 564, 581, 606, 628, 666, 780, 978 nm | VNIR-HSI | crossbreed: every hour Uckermarker: 0, 20, 40, 60, 90, 120 min and then hourly | VIP-PLSR | R = 0.96 | von Gersdorff et al. (2021) |
| Dry-cured pork | MC | AD | Temp.: 50 °C | 400-1000 nm | 440, 445, 460, 494, 545, 555, 580, 585, 630, 636, 676, 780, 925, 954, 956, 980 nm | VNIR-HSI | 5, 10, 15, 20 h | CARS-PLSR | $R^2_p$ = 0.926 RMSEP = 0.121 | Tian, Aheto, Dai, et al. (2021) |
| Fermented sausage | Classification | AD | Temp.: 55, 15 °C RH: 80, 65% | 950-1650 nm | 930-1300, 1150-1200, 1370-1650 nm | portable NIRS | 0, 12, 24, 36, 48, 60, 120 h | PCA , K-NN, PLS-DA | CCR = 100% Specificity = 1 sensitivity = 1 | Gonzalez-Mohino et al. (2020) |
| Gingers slices | MC | MVD | Power: 250 W Pressure: 20 mbar | 950-1655 nm | 1105, 1124, 1152, 1204, 1282, 1340, 1370, 1422, 1558 nm | NIR-HSI | 0, 25, 40, 55, 80 min | RC-PLSR | $R^2_p$ = 0.973 RMSEP = 4.63% | Lin, Xu, and Sun (2020b) |
| Gingers slices | MC | AD | Temp.: 60 °C | 950-1655 nm | – | NIR-HSI | 0, 3, 4.5, 5.5, 6.5 h | PLSR | $R^2_p$ = 0.96 RMSEP = 5.74% | Lin and Sun (2020b) |

| | | | | | | | | | | |
|---|---|---|---|---|---|---|---|---|---|---|
| Gingers slices | MC Classification | HAD, MVD | Temp.: 60 °C Power: 250 W Pressure: 2 kPa | 950-1655 nm | MC: 1008, 1155, 1193, 1351, 1406, 1442, 1569 nm Classification: 1025, 1116, 1190, 1348, 1414, 1500, 1204, 1287, 1425 nm | NIR-HSI | MVD: 25, 40, 55, 80 min HAD: 3, 4.5, 5.5, 6.5 h | RCV-PLSR PCA, variograms,SVM | $R^2_p$ = 0.971 RMSEP = 5.02% CCR = 90.3% | Lin, Xu, and Sun (2020a) |
| Grass carp fillets | MC | VFD | Temp.: −56 °C Pressure: 10 Pa | 400-1000 nm | 416, 466, 501, 553, 567, 583, 607, 621, 956, 997 nm | VNIR-HSI | 3, 6, 12, 18, 24, 30, 36 h | RC-PLSR | $R^2_p$ = 0.9325 RMSEP = 5.34% | Ma, Qu, and Sun (2017) |
| Grass carp slices | MC | VFD | Temp.: −56 °C Pressure: 10 Pa | 400-1000 nm | 414, 490, 520, 563, 580, 593, 634, 709, 972 nm | VNIR-HSI | 1, 3, 6, 12, 18, 24, 30, 36 h | Modifid RC-PLSR | $R^2_p$ = 0.9117 RMSEP = 56.3 g/kg | Qu et al. (2017) |
| Pork | MC | H-D, CAD | Temp. (H-D): 50 °C Temp. (CAD): −18 °C | 400-1000 nm | 424, 443, 541, 589, 607, 724, 937 nm | VNIR-HSI | 60, 120, 180 min | Modifid RC-PLSR | $R^2_p$ = 0.9489 RMSEP = 1.4736 | Ma, Sun, and Pu (2017) |
| Hops | MC | AD | Temp.: 65, 70 °C Air velocity: 0.15, 0.35 m/s | 400-1000 nm | 658, 664, 839, 901, 920, 1010 nm | VNIR-HSI | 15, 25, 35, 45, 75 min and then every 30 min | MCUVE-PLSR | $R^2_p$ = 0.95 RMSEP = 0.24 | Sturm et al. (2020) |
| Maize kernel | MC, MCU | PSMVD | Pressure: 7-10 kPa Power: 516 W Spout: 5 s interval, 3 s hold | 400-1000 nm | – | VNIR-HSI | 10, 20, 30, 40, 50, 60 min | PLSR | $R^2_p$ = 0.992 (MC) $R^2_p$ = 0.848 (MCU) RMSEP = 2.88% (MC) RMSEP = 2.73 (MCU) | Huang et al. (2015) |
| Mango slices | MC | MVD | Power: 250 W Pressure: 20 mbar Cycle: 1 min on, 2 min off | 400-1000 nm 880-1720 nm | 908, 1076, 1153, 1405, 1706 nm | VNIR-HSI, NIR-HSI | 0, 3, 6, 9, 12, 15, 20, 25, 30 min | RC-PLSR | $R^2_p$ = 0.972 RMSEP = 4.611% | Pu and Sun (2015) |
| Mango slices | MC | MVD | Pressure: 20 mbar Power: 250 W Cycle: 1 min on, 2 min off | 880-1720 nm | 951, 977, 1138, 1362, 1386, 1420, 1440 nm | NIR-HSI | 0, 3, 6, 9, 12, 15, 18, 30 min | RCV-MLR | $R^2_p$ = 0.993 RMSEP = 1.282% | Pu and Sun (2016) |
| Mango slices | MC | HAD, MVD, HAD + MVD. | Temp. (HAD): 60 °C Power (MVD): 250 W Pressure (MVD): 20 mbar | 880-1720 nm | – | NIR-HSI | MVD: 0, 3, 6, 9, 12, 15, 20, 25 min AD: 0, 1, 2, 3, 4, 5, 6, 7, 8, 9, 10, 11 h Combination: 0 h, 4 h, 4 h 8 min | PLSR | $R^2_p$ = 0.995 RMSEP = 1.408% | Pu and Sun (2017) |
| Melon slices | MC | AD | Temp.: 60 °C | 1000-2500 nm | – | NIR-HSI | 0, 15, 30, 45, 60, 90, 120, 150, 180, 210 min | PLSR | $R^2_p$ = 0.990 RMSEP = 2.9794% | Netto et al. (2021) |
| Mushroom cubes | MC | HAD | Temp.: 60 °C | 405-970 nm | 405, 435, 450, 470, 505, 525, 570, 590, 630, 645, 660, 700, | VNIR-MSI | 0, 120, 180, 240, 360, 420 min | BPNN | $R^2_p$ = 0.9639 RMSEP = 0.2291% | Younas et al. (2020) |

(*continued*)

**TABLE 2.** Continued.

| Samples | Quality indicators | Dehydration methods | Conditions | Spectral ranges | Critical wavelengths | Spectral techniques | Monitor schedules | Models | Best Results | References |
|---|---|---|---|---|---|---|---|---|---|---|
| | | | | | 780, 850, 870, 890, 910, 940, 970 nm | | | | | |
| Mushroom | MC | MVD | Power: 250 W Pressure: 2 kPa Heating cycle: 4 min on + 1min off (whole); 2 min on + 1min off (slices) | 950-1655 nm | – | NIR-HSI | Whole: 0, 10, 20, 30, 40, 50, 60 min Slices: 0, 6, 12, 18, 24, 30, 39, 48 min | PLSR | $R^2_p$ = 0.985 (Slice) $R^2_p$ = 0.963 (Whole) RMSEP = 4.285% (Slice) RMSEP = 10.04% (Whole) | Lin, Xu, and Sun (2019) |
| Organic apples slices | MC | AD | Temp.: 60, 70 °C | 500-1010 nm | 580, 750, 970 nm | VNIR-HSI | 60 °C: 0, 15, 30, 60, 90, 120, 180, 240, 300, 360 min 70 °C: 0, 15, 30, 60, 90, 120, 150, 180, 210, 240 min | RV-PLSR | $R^2_p$ = 0.98 RMSEP = 0.27 | Shrestha et al. (2018) |
| Persimmons | MC | HAD | Temp.: 40 °C Cycle: 12 h on, 12 h off | 900-2500 nm | – | SWIR-HSI | 0, 1, 2, 3, 4, 5, 6 days | PLSR | $R^2_p$ = 0.9494 RMSEP = 2.1857% | Cho, Choi, and Moon (2020) |
| Pistachi kernels | MC | AD | Temp.: 90, 120, 150 °C Air velocities: 0.5, 1.5, 2.5 m/s | 400-1000 nm | – | VNIR-HSI | 20, 35, 50 min | ANN | $R^2_p$ = 0.907 RMSEP = 0.179 | Mohammadi-Moghaddam et al. (2018) |
| Pork slices | MC | H-D, B-D | Temp. 50 °C (H-D), 20 °C (B-D) B-D salt: 30% NaCl (w/w) | 328-1115 nm | 411, 454, 591, 650, 740, 915 nm | VNIR-HSI | H-D: 60, 120, 180 min B-D: 90, 180, 300 min | Optimized RC-PLSR | $R^2_p$ = 0.996 RMSEP = 0.855 | Ma, Sun, and Pu (2016) |
| Potato and sweet potato slices | MC | AD, MD | Temp. (AD): 80 °C Power (MD): 600 W | 10372-6105, 3996-600, 1700-900 $cm^{-1}$ | 1014, 1071, 1138, 1212, 1326, 1366, 1406, 1436, 1520 nm | NIR-HSI, MIR-HSI | AD: 30, 60, 90, 150, 210 min MD: 15, 30, 45, 60, 80 s | RC-BPANN | $R^2_p$ = 0.965 RMSEP = 0.023 | Su, Bakalis, and Sun (2019b) |
| Potato and sweet Potato slices | MC | AD, MD | Temp. (AD): 80 °C Power (MD): 600 W | 10372-6105, 3996-600, 1700-900 $cm^{-1}$ | – | NIR-HSI, MIR-HSI | AD: 30, 60, 90, 150, 210 min MD: 15, 30, 45, 60, 80 s | LWPLSR | $R^2_p$ = 0.987 RMSEP = 0.015 | Su, Bakalis, and Sun (2019a) |
| Potato slices | MC | AD | Temp.: 50, 60, 70 °C | 500-1000 nm | 500, 516, 583, 701, 949, 972 nm | VNIR-HSI | Every 30 min | Modifid-PLSR | $R^2_p$ = 0.95 RMSEP = 0.25 | Amjad et al. (2018) |
| Potato slices | MC | AD | Temp.: 50 °C | 500-1010 nm | 6 features subset | VNIR-HSI | Every 30 min | iPLS | $R^2_p$ = 0.948 RMSEP = 0.26 | Moscetti, Sturm, et al. (2018) |
| Prawns | MC | AD | Temp.: 40 °C | 380-1100 nm | 428, 445, 544, 569, 629, 672, 697, 760, 827, 917, 958, 999 nm | VNIR-HSI | 0, 30, 70, 110, 150, 200 min | SPA-MLR | $R^2_p$ = 0.962 RMSEP = 4.997 | Wu, Shi, et al. (2012) |
| PFSP slices | MC, FWC | CUHAD | Power: 60 W Frequency: 29 kHz Temp.: 40 °C | 371-1023 nm | MC: 623, 642, 646, 703, 709, 726, 817, 840, 885, 957 nm | VNIR-HSI | 0, 30, 60, 120, 180, 240 min | RC-MLR | $R^2_p$ = 0.9359 (MC) $R^2_p$ = 0.8592 (FWC) RMSEP = 2.8583% | Sun et al. (2017) |

| | | | | | | | | | | |
|---|---|---|---|---|---|---|---|---|---|---|
| | | | Air velocity: 1 m/s | | FWC: 623, 636, 646, 708, 726, 817, 840, 885, 958 nm | | | | (MC) RMSEP = 0.0463 (FWC) | |
| Purple sweet potatoes | MC | HAD, MD | Temp. (HAD): 80 °C Air velocity (HAD): 2 m/s Power (MD): 700 W | 400-1000 nm | HAD: 447, 562, 618, 709, 854, 862, 870, 904, 915, 918, 935 nm MD: 441, 448, 576, 616, 781, 850, 855, 921, 923, 960 nm | VNIR-HSI | HAD: 20, 45, 60, 120 min MD: 1, 2, 5, 8 min | CARS-PLSR | $R^2_p$ = 0.862 (HAD) $R^2_p$ = 0.867 (MD) RMSEP = 0.079 (HAD) RMSEP = 0.088 (MD) | Tian, Aheto, Dai, et al. (2021) |
| Radish slabs | MC | HAD, MWD, HAD + MWD | Temp. (HAD): 70 °C Air velocity (HAD): 5 m/s Power (MWD): 50 W | 894-2504 nm | 38 variables | NIR-HSI | HAD: Every 15 min from 0-135 min MWD: Every 5 min from 0-50 min Combine: Every 5 min from 0-45 min | VIP- RLSR | $R^2_{val}$ = 0.962 RMSEC = 4.45% | Lee et al. (2020) |
| Boiled scallops | MC | HAD | Temp.: 55 °C Cycle: 20 h on; 4 h on + 1 h off + 15 h on; 6 h on + 1 h off + 13 h on | 387.1-1024.7 nm | 405.7, 513.2, 606.9, 967.1 nm | VNIR-HSI | 0, 1, 2, 3, 4, 5, 6, 7, 8, 10, 12, 16, 20 h | RC-PLSR | $R^2_p$ = 0.9662 RMSEP = 0.0353 | Sun et al. (2020) |
| Scallops | MC | AD | Temp.: 105 °C | 380-1030 nm | 440, 497, 535, 574, 728, 910, 955, 1022 nm | VNIR-HSI | 10, 20, 30, 40, 50, 60 min | RC-PLSR | $R^2_p$ = 0.9673 RMSEP = 3.5584% | Huang et al. (2017) |
| Shiitake mushrooms | Water fractions | FIR Drying | Temp.: 70 °C | 405-970 nm | 405, 435, 450, 470, 505, 525, 570, 590, 630, 645, 660, 700, 780, 850, 870, 890, 910, 940, 970 nm | VNIR-MSI | 0, 30, 60, 120, 180, 240 min | PLS | $R^2_p$ = 0.95 (free water) $R^2_p$ = 0.92 (immobilised water) $R^2_p$ = 0.83 (bound water) RMSEP = 8.09% (free water) RMSEP = 8.00% (immobilised water) RMSEP = 4.95% (bound water) | Younas, Mao, Liu, Liu, et al. (2021) |
| Shiitake mushroom | Water fractions | FD | Temp.: −50 °C Pressure: 1 Pa | 405-970 nm | 405, 435, 450, 470, 505, 525, 570, 590, 630, 645, 660, 700, 780, 850, 870, 890, 910, 940, 970 nm | VNIR-MSI | 0, 3, 6, 12, 24, 36 h | LS-SVM | $R^2_p$ = 0.85 (free water) $R^2_p$ = 0.90 (immobilised water) $R^2_p$ = 0.88 (bound water) $R^2_p$ = 0.87 (total water) RMSEP = 12.61% (free water) RMSEP = 7.10% (immobilised water) RMSEP = 18.13% (bound water) | Younas, Mao, Liu, Murtaza, et al. (2021) |

(*continued*)

**TABLE 2.** Continued.

| Samples | Quality indicators | Dehydration methods | Conditions | Spectral ranges | Critical wavelengths | Spectral techniques | Monitor schedules | Models | Best Results | References |
|---|---|---|---|---|---|---|---|---|---|---|
| | | | | | | | | | RMSEP = 4.55% (total water) | |
| Sodium caseinate film | MC | Natural Dehydration | Temp.: 23 °C RH: 45% | 880-1720 nm | – | NIR-HSI | Set 1: 24, 27, 30, 35, 46, 50 h, Set 2, 3: 24, 27, 30, 48 h | SVM | $R^2_p$ = 0.97 RMSEP = 0.056 | Xu, Gowen, and Sun (2018) |
| Tea leaves | MC | AD | Temp.: 80 °C | 380-1030 nm | 542, 709, 752, 971 nm | VNIR-HSI | 0, 3, 10, 30 min | SPA-PLSR PCA-LDA | $R^2_p$ = 0.946 RMSEP = 0.052 CCR = 76.923%-100% | Xie et al. (2013) |
| Vegetable soybean | MC | PSMVD | – | 400-1000 nm | 457.96, 509.48, 567.44, 586.76, 612.52, 657.6, 696.24, 747.76, 773.52, 850.8, 908.76, 934.52 nm | VNIR-HSI | 0, 10, 20, 30, 40, 50, 60, 70, 80 min | BFWA-PLSR; | $R^2_p$ = 0.966 RMSEP = 5.105% | Yu et al. (2019) |
| Vegetable soybean | MC | PSMVD | Pressure: 9 kPa Power: 516 W Spout:: 1 s interval, 3 s hold | 400-1000 nm | – | NIR-HSI | 0, 10, 20, 30, 40, 50, 60, 70, 80 min | Modified PLSR | $R^2_p$ = 0.973 RMSEP = 4.6% | Huang et al. (2014) |
| Carrot slices | MC | HAD | Temp.: 60 °C | 405-970 nm | 405, 435, 450, 470, 505, 525, 570, 590, 630, 645, 660, 700, 780, 850, 870, 890, 910, 940, 970 nm | NIR-MSI | 0, 30, 60, 120, 180, 240, 300 min | BPNN | $R^2_p$ = 0.991 RMSEP = 1.482% RPD = 11.378 | Liu et al. (2016) |
| Apple slice | MC | HAD | Temp.: 65 °C | 740-1700 nm | – | NIRS | 0, 1, 2, 3, 4, 5, 6, 7 h | PLSR | r = 0.988 RMSEP = 24.82 | Dénes et al. (2012) |
| Beef lump | $a_w$ | AD | Temp.: 4 °C RH: 80% | 700-1050 nm | – | NIRS | Arbitary interval in 27 days | PLSR | $R^2$ = 0.81, RMSE = 0.34 g/g-d.s | Ishikawa, Ueno, and Fujii (2017) |
| Dry-Cured ham | MC, $a_w$ | AD | Temp.: 4, 12-14, 16-18, 18-20 °C RH: 60-70% | 833-2500 nm | – | FT-NIRS | 4, 7, 11, 15, 19, 22, 26, 30, 36 weeks | PLSR | $R^2$ = 0.93 (MC) $R^2$ = 0.62 ($a_w$) RMSEV = 3.51 (MC) RMSEV = 0.0141 ($a_w$) RPD = 3.74 (MC) RPD = 1.63 ($a_w$) | Collell et al. (2011) |
| Edible coating on bread | MC | AD | Temp.: 25, 60 °C RH: 50%, 10% | 833-2500 nm | – | NIRS | 25 °C, 1 layer: every 30 min 60 °C, 1 layer: every 15 min 60 °C, 3 layers: every 10 min | PCA, PLS | $R^2$ = 0.963 (top) RMSET = 2.87% (top) $R^2$ = 0.937 (bottom) RMSECV = 3.15% (bottom) | Chakravartula et al. (2019) |
| Fermented sausages | MC, $a_w$ | AD | Temp.: 12, 14, 16 °C RH: 80%, 65%, | 830-2500, 920-1800, 1100-2300 nm | – | FT-NIRS, Portable NIRS, AOTF-NIRS | set 1: 0, 2, 4, 7, 9, 11, 14, 16, 18 days. set 2: 0, 2, 4, 7, | PCA, PLSR | $R^2_p$ = 0.990 (MC) $R^2_p$ = 0.984 ($a_w$) RMSEP = 1.560% (MC) | Collell et al. (2012) |

| | | | | | | | | | | |
|---|---|---|---|---|---|---|---|---|---|---|
| | | | 72%, 78.5%, 90.8% | | | | 9, 11, 14, 16, 18, 21, 23, 25, 28, 30, 32, 35, 37, 39 days set 3: 0, 2, 5, 10, 20, 25, 35, 51, 68 days | | RMSEP = 0.007% ($a_w$) | |
| Fresh blueberry | MC | PS-MFD | Microwave density: 3 W/g Spouting: 20 min interval, 0.3 s hold | 900-1599 nm | – | NIRS | Every 30 min | BPANN | $R^2$ = 0.9951 | Liu et al. (2021) |
| Intact macadamia nuts | MC | AD | Temp.: 30, 40, 60 °C | 866-2530 nm | – | NIRS | 0, 4, 6, 7 days | PLS | $R^2_C$ = 0.66 RMSEP = 3.23 SEP = 3.26 meq/kg | Carvalho, Leite, et al. (2019) |
| Mango slices | MC | Soalr Drying | Temp.: 16.8–54.3 °C RH: 19.2–99.3% | 285-1200 nm | 648–747, 849–948 nm | portable VNIRS | 9:00, 13:00, 17:00 for 3 days | PCA, PLSR | $R^2_p$ = 0.940 RMSEP = 5.19% w/w RPD = 4.04 | Wokadala et al. (2020) |
| Organic apple wedges | MC, $a_w$, classification | HAD | Temp.: 60 °C | 1100-2300 nm | $a_w$: 1144, 1496, 1876, 2118, 2166, 2290 nm MC: 1330, 1878 nm Classification: 1548, 1852, 2146, 2184 nm | portable AOTF-NIRS | 0, 1, 2, 3, 4, 5, 6, 7, 8 h | iPLS, K-means, iPLS-DA | $R^2_p$ = 0.98 ($a_W$) $R^2_p$ = 0.98 (MC) RMSEP = 0.03 ($a_W$) RMSEP = 0.04 (MC) CCR = 0.90-0.98 | Moscetti, Raponi, et al. (2018) |
| Organic carrot slices | MC, $a_w$, classification | HAD | Temp.: 40 °C | 1100-2300 nm | $a_w$: 1134, 1408, 1724, 2166, 2224 nm MC: 1100, 1396, 1558, 1726, 1930 nm Classification: 1376, 1386, 1540, 1980, 2042, 2264 nm | AOTF-NIRS | 0, 1, 2, 3, 4, 5, 6, 7, 8 h | iPLS K-means, iPLS-DA | $R^2_p$ = 0.96 ($a_W$) $R^2_p$ = 0.98 (MC) RMSEP = 0.04 ($a_W$) RMSEP = 0.03 (MC) CCR = 0.90-0.97 | Moscetti et al. (2017) |
| ODP | MC, $a_w$ | HAD | Temp.: 60 °C | 800-2400 nm | $a_w$: 916-1100, 1412-1620, 1910-2138 nm MC: 916-1132, 1382-1636, 1880-2056 nm | NIRS | 2, 4, 6, 8, 10, 12 h | SCMWPLSR | $R^2_p$ = 0.993 ($a_W$) $R^2_p$ = 0.994 (MC) RMSEP = 0.014 ($a_W$) RMSEP = 0.69% (MC) | Rongtong et al. (2018) |
| Aqueous sucrose solutions | MC | FD | Temp.: −23, 30 °C Pressure: 55 mTorr | 970-2500 nm | – | Multipoint-NIRS | every second with 15 ms integration time | PCA, PLSR | $R^2_p$ = 0.793 (all) $R^2_p$ = 0.876 (146 mM) $R^2_p$ = 0.928 (584 mM) RMSEP = 0.270% (all) RMSEP = 0.037% (146 mM) RMSEP = 0.125% (584 mM) | Kauppinen et al. (2013) |
| Pork sausages | MC, $a_w$ | AD | Temp.: 12 °C Air velocity: | 833-2500 nm | – | FT-NIRS | twice during fermentation, | PLSR | $R^2_p$ = 0.998 (MC) $R^2_p$ = 0.988 ($a_w$) | Collell et al. (2010) |

(*continued*)

**TABLE 2.** Continued.

| Samples | Quality indicators | Dehydration methods | Conditions | Spectral ranges | Critical wavelengths | Spectral techniques | Monitor schedules | Models | Best Results | References |
|---|---|---|---|---|---|---|---|---|---|---|
| | | | 0.5 m/s RH: 58.6%-90.8% | | | | seven times during drying | | RMSEP = 0.622 (MC) RMSEP = 0.006 ($a_w$) | |
| Pasta | MC | AD | Temp.: 40-105 °C RH: 40%-95% | – | | MIRS, NIRS, Raman | thrice during process | PLSR | R = 0.998 (MIR) R = 0.997 (NIR) R = 0.991 (Raman) | Czaja et al. (2018) |
| Pork muscles | MC | H-D | Temp.: 90 °C | 0.1-0.9 THz | – | THz-TDS | 5, 10, 25, 40, 120 min | Landau-Looyenga-Lifshitz | $\Delta C$ = 6% | Borovkova et al. (2018) |
| Pot herbs | MC, Permittivity | Natural dehydration | Temp.: 18 °C RH: 30% | 0.75-1.1 THz | – | THz-TDS | Every 2 hours | NRW | "Strong correlation" | Zahid et al. (2019) |
| **Chromaticity evaluation** | | | | | | | | | | |
| Apple slices | a*, b* | AD | Temp.: 50, 70 °C | 400-1010 nm | a*: 543 and 966 nm b*: 510, 664, 714, 914, 969 nm | VNIR-HSI | 0, 30, 60, 90, 120, 150, 180, 240, 300 min | PLSR | $R^2_p$ = 0.96 (a*) $R^2_p$ = 0.80 (b*) RMSEP = 0.33 (a*) RMSEP = 0.31 (b*) | Crichton et al. (2018) |
| Banana slices | a*, b*, L* | AD | Temp.: 90 °C | 400-1000 nm | – | cross-polarized VNIR-HSI | 0, 30, 60, 90, 120, 150, 180, 210 min | PLSR | $R^2_p$ = 0.53 (a*) $R^2_p$ = 0.83 (b*) $R^2_p$ = 0.61 (L*) RMSEP = 1.32 (a*) RMSEP = 1.95 (b*) RMSEP = 5.92 (L*) | Nguyen-Do-Trong, Dusabumuremyi, and Saeys (2018) |
| Beef slices | a*, b* | AD | Temp.: 70 °C | 400-1010 nm | a*: 501, 545, 599, 600, 609, 620, 639, 876 nm b*: 513, 552, 574, 575, 580, 583 nm | VNIR-HSI | 1, 2, 3, 4, 5, 6 h | CARS-PLSR (a*) MCUVE-PLSR (b*) | $R^2_p$ = 0.98 (a*) $R^2_p$ = 0.98 (b*) RMSEP = 0.91 (a*) RMSEP = 0.42 (b*) | von Gersdorff et al. (2018) |
| Beef slices | a*, b*, L* | AD | Temp.: 68 °C | 400-1010 nm | a*: 501, 545, 599, 600, 609, 620, 639, 876, 938, 959, 961, 977, 987, 995 nm b*: 498, 513, 525, 557, 670, 678, 679, 790, 828, 915, 946, 957 nm L*: 516, 695, 823, 917, 957, 959, 961, 967, 969, 985 nm | VNIR-HSI | 1, 2, 3, 4, 5, 6 h | CARS-PLSR | $R^2_p$ = 0.98 (a*) $R^2_p$ = 0.96 (b*) $R^2_p$ = 0.96 (L*) RMSEP = 0.91 (a*) RMSEP = 0.70 (b*) RMSEP = 1.09 (L*) | Retz et al. (2017) |
| Beef slices | a*, b*, L* | MD | Power: 500 W | 400-1000 nm | a*: 402, 485, 553, 586, 623, 678, 785, 946 nm | VNIR-HSI | 0, 30, 45, 60, 75 s | RC-MLR (a*), LS-SVM (b*), PLSR (L*) | $R^2_p$ = 0.890 (a*) $R^2_p$ = 0.816 (b*) $R^2_p$ = 0.887 (L*) RMSEP = 0.735 (a*) RMSEP = 0.521 (b*) RMSEP = 0.741 | Liu et al. (2018) |

| | | | | | | | | | | |
|---|---|---|---|---|---|---|---|---|---|---|
| | | | | | | | | | (L*)<br>RPD = 2.733 (a*)<br>RPD = 2.054 (b*)<br>RPD = 2.569 (L*) | |
| Beef slices | a*, b*, L* | HAD | Temp.: 50, 60, 70 °C<br>Air velocity: 0.6 m/s | 500-1009 nm | 500, 518, 543, 564, 581, 606, 628, 666, 780, 978 nm | VNIR-HSI | crossbreed: every hour<br>Uckermarker: 0, 20, 40, 60, 90, 120 min and then hourly | VIP-PLSR | R = 0.99 (a*)<br>R = 0.98 (b*)<br>R = 0.97 (L*) | von Gersdorff et al. (2021) |
| Hops | a*, b* | AD | Temp.: 65, 70 °C<br>Air velocity: 0.35, 0.15 m/s | 400-1000 nm | a*: 620, 665, 902, 912, 1010 nm<br>b*: 531, 758, 764, 766, 777, 784, 785, 806, 899, 912, 928, 938, 980 nm | VNIR-HSI | 15, 25, 35, 45, 75 min and then every 30 min | MCUVE-PLS (a*), CARS-PLS (b*) | $R^2_p$ = 0.81 (a*)<br>$R^2_p$ = 0.73 (b*)<br>RMSEP = 2.79 (a*)<br>RMSEP = 1.94 (b*) | Sturm et al. (2020) |
| Organic apples slices | a*/b* | AD | Temp.: 60, 70 °C | 500-1010 nm | 580 and 680 nm | VNIR-HSI | 60 °C: 0, 15, 30, 60, 90, 120, 180, 240, 300, 360 min<br>70 °C: 0, 15, 30, 60, 90, 120, 150, 180, 210, 240 min | RV-PLSR | $R^2_p$ = 0.82 (a*/b*)<br>RMSEP = 0.23 (a*/b*) | Shrestha et al. (2018) |
| Potato slices | a*, b* | AD | Temp.: 50, 60, 70 °C | 500-1000 nm | a*: 508, 520, 633, 675, 956, 974 nm<br>b*: 501, 514, 549, 741, 878, 966 nm | VNIR-HSI | Every 30 min | PLS | $R^2_p$ = 0.83 (a*)<br>$R^2_p$ = 0.83 (b*)<br>RMSEP = 0.84 (a*)<br>RMSEP = 2.89 (b*) | Amjad et al. (2018) |
| Potato slices | hue, $L^*b^{*-1}$ | AD | Temp.: 50 °C | 500-1010 nm | 4 and 6 feature subsets of wavelengths for h and $L^*b^{*-1}$ | VNIR-HSI | Every 30 min | iPLS | $R^2_p$ = 0.932 (h)<br>$R^2_p$ = 0.895 ($L^*b^{*-1}$)<br>RMSEP = 1.22 (h)<br>RMSEP = 0.1 ($L^*b^{*-1}$) | Moscetti, Sturm, et al. (2018) |
| Tea leaves | $\Delta L^*$, $\Delta a^*$, $\Delta b^*$, classification | AD | Temp.: 80 °C | 380-1030 nm | Δ a*: 540, 608, 676, 690, 985, 1017 nm<br>Δ b*: 404, 408, 414, 416, 418, 444, 540, 648, 770, 866, 971 nm<br>Δ L*: 457, 540, 649, 735, 761, 874, 1017 nm | VNIR-HSI | 0, 4, 6, 8, 10 min | SPA-LS-SVM | $R^2_p$ = 0.849 (a*)<br>$R^2_p$ = 0.917 (b*)<br>$R^2_p$ = 0.929 (L*)<br>RMSEP = 1.146 (a*)<br>RMSEP = 2.142 (b*)<br>RMSEP = 1.178 (L*)<br>CCR = 71.43%-100% | Xie et al. (2014) |
| Vegetable soybean | $\Delta E$ | PSMVD | Pressure: 9 kPa<br>Power: 516 W<br>Spout: 1 s interval, 3 s hold | 400-1000 nm | – | VNIR-HSI | 0, 10, 20, 30, 40, 50, 60, 70, 80 min | PLSR | $R^2_p$ = 0.862<br>PMSEP = 1.04 | Huang et al. (2014) |
| Organic apple wedges | C* | HAD | Temp.: 60 °C | 1100-2300 nm | 1156, 1630, 2180, 2244 nm | poratble AOTF-NIRS | 0, 1, 2, 3, 4, 5, 6, 7, 8 h | iPLS | $R^2_p$ = 0.86<br>RMSEP = 2.33 | Moscetti, Raponi, et al. (2018) |
| | L*, h | HAD | Temp.: 40 °C | 1100-2300 nm | | AOTF-NIRS | | iPLS | | Moscetti et al. (2017) |

(*continued*)

**TABLE 2.** Continued.

| Samples | Quality indicators | Dehydration methods | Conditions | Spectral ranges | Critical wavelengths | Spectral techniques | Monitor schedules | Models | Best Results | References |
|---|---|---|---|---|---|---|---|---|---|---|
| Organic carrot slices | | | | | L*: 1292, 1548, 1778, 1842, 2042, 2160, 2250, 2286 nm h: 1316, 1372, 1544, 2186, 2236, 2256, 2270, 2278 nm | | 0, 1, 2, 3, 4, 5, 6, 7, 8 h | | $R^2_p$ = 0.83 (L*) $R^2_p$ = 0.87 (h) RMSEP = 1.66 (L*) RMSEP = 1.34 (h) | |
| **Texture evaluation** | | | | | | | | | | |
| Banana slices | Texture | AD | Temp.: 90 °C | 400-1000 nm | – | cross-polarized VNIR-HSI | 0, 30, 60, 90, 120, 150, 180, 210 min | PLSR | $R^2_p$ = 0.66 RMSEP = 11.8 N | Nguyen-Do-Trong, Dusabumuremyi, and Saeys (2018) |
| Banana slices | Hardness, Fracturability | MVD | Power: 250 W Pressure: 2000 Pa | 950-1650 nm | – | NIR-HSI | 3, 6, 9, 10, 12, 14, 15, 18, 19, 21 min | SVMR | $R^2_p$ = 0.927 (hardness) $R^2_p$ = 0.961 (fracturability) RMSEP = 3.700 N (hardness) RMSEP = 0.847 mm (fracturablility) | Pu et al. (2018) |
| Pistachi kernels | Fracture force, Compressive energy, elasticity, hardness | AD | Temp.: 90, 120, 150 °C Air velocities: 0.5, 1.5, 2.5 m/s | 400-1000 nm | – | VNIR-HSI | 20, 35, 50 min | ANN | $R^2_p$ = 0.957 (fracture force) $R^2_p$ = 0.907 (compressive energy) $R^2_p$ = 0.921 (elasticity) $R^2_p$ = 0.876 (hardness) RMSEP = 3.386 N (fracture force) RMSEP = 15.757 N.MM (compressive energy) RMSEP = 2.366 N/s (elasticity) RMSEP = 5.216 N (hardness) | Mohammadi-Moghaddam et al. (2018) |
| Grass carp fillets | WBSF, hardness, gumminess, chewiness | VFD | Temp.: −56 °C Pressure: 10 Pa | 400-1000 nm | 555, 569, 585, 607, 619, 643, 782, 915, 953, 995 nm | VNIR-HSI | 3, 6, 12, 18, 24, 30, 36 h | RC-PLSR | $R^2_p$ = 0.8774 (WBSF) $R^2_p$ = 0.8523 (hardness) $R^2_p$ = 0.7982 (gumminess) $R^2_p$ = 0.8453 (chewiness) RMSEP = 16.12 N (WBSF) RMSEP = 21.37 N (hardness) RMSEP = 14.54 N | Ma et al. (2017) |

| | | | | | | | | | | |
|---|---|---|---|---|---|---|---|---|---|---|
| | | | | | | | | | (gumminess) RMSEP = 7.25 N (chewiness) | |
| Tuber | Hardness, resilience, springiness, cohesiveness, gumminess, chewiness | Microwave baking | Power: 800 W | 4000-600 $cm^{-1}$ | Set1:1350, 1221, 1083, 1026, 985, 924 nm Set2:1468, 1333, 1221, 1026, 985, 924 nm Set3:1468, 1333, 1083, 1026, 985, 924 nm | FTMIR-ATR | 0, 10, 20, 30, 35 s | FMCIA-SPA-LWPLSR | $R^2_p$ = 0.797 (hardness) $R^2_p$ = 0.881 (resilience) $R^2_p$ = 0.584 (springiness) $R^2_p$ = 0.574 (cohesiveness) $R^2_p$ = 0.728 (gumminess) $R^2_p$ = 0.690 (chewiness) | Su, Bakalis, and Sun (2018) |
| Tuber | UCS | Microwave baking | Power: 800 W | 4000-600 $cm^{-1}$ | – | FTMIR-ATR | 0, 10, 15, 20, 35, 30, 35, 40 s | SVMR | $R^2_p$ = 0.752 RMSEP = 0.217 | Su, Bakalis, and Sun (2019c) |
| **Rehydration property evaluation** | | | | | | | | | | |
| Grass carp fillets | Rehydrating mass gain percentage | VFD | Temp.: −56 °C Pressure: 10 Pa | 400-1000 nm | 419, 443, 610, 645, 665, 708, 760, 811, 951 nm | VNIR-HSI | 3, 6, 12, 18, 24, 30, 36 h | RC-PLSR | $R^2_p$ = 0.8278 RMSEP = 9.79% | Ma, Qu, and Sun (2017) |
| Gingers slices | Rehydration rates | AD | Temp.: 60 °C | 950-1655 nm | – | NIR-HSI | 5, 10, 15, 20, 30, 40, 50, 60, 80, 100, 120, 150, 180 min | PLSR | $R^2_p$ = 0.957 RMSEP = 29.20% | Lin and Sun (2020b) |
| **Chemical content evaluation** | | | | | | | | | | |
| Hops | Aromatic component | AD | Temp.: 65, 70 °C Air velocity: 0.35, 0.15 m/s | 400-1000 nm | Myrcene: 505, 554, 575, 605, 690, 883, 931, 941, 946, 971, 1010 nm $\beta$-Ocimen: 507, 557, 651, 659, 920, 946, 951, 1010 nm 1-octen-3-ol: 517, 536, 575, 580, 659, 1010 nm | VNIR-HSI | 15, 25, 35, 45, 75 min and then every 30 min | MCUVE-PLS | $R^2_p$ = 0.83 (Myrcene) $R^2_p$ = 0.73 ($\beta$-Ocimen) $R^2_p$ = 0.64 (1-octen-3-ol) RMSEP = $3.83 \times 10^7$ (Myrcene) RMSEP = $4.61 \times 10^6$ ($\beta$-Ocimen) RMSEP = $5.24 \times 10^4$ (1-octen-3-ol) | Sturm et al. (2020) |
| PFSP slices | Anthocyanin content | CUHAD | Temp.: 40 °C Air velocity: 1 m/s ultrasound power: 60 W ultrasound frequency: 28 kHz | 371-1023 nm | 637, 660, 666, 700, 729, 761, 801, 837, 892, 957 nm | VNIR-HSI | 0, 0.5, 1, 2, 3, 4, 5, 6, 7 h | RC-MLR | $R^2_p$ = 0.866 RMSEP = 0.302 mg/g | Liu et al. (2017) |
| Purple sweet potatoes | Total anthocyanin | HAD, MD | Temp.: 80 °C Air velocity: 2 m/s Microwave power: 700 W | 400-1000 nm | HAD: 450, 465, 484, 566, 589, 709, 722, 854, 868 nm MD: 443, 445, 450, 455, 463, 783, 855, 912, | VNIR-HSI | HAD: 20, 45, 60, 120 min MD: 1, 2, 5, 8 min | CARS-PLSR | $R^2_p$ = 0.847 (HAD) $R^2_p$ = 0.859 (MD) RMSEP = 0.303 (HAD) RMSEP = 0.241 (MD) | Tian, Aheto, Dai, et al. (2021) |

(*continued*)

**TABLE 2.** Continued.

| Samples | Quality indicators | Dehydration methods | Conditions | Spectral ranges | Critical wavelengths | Spectral techniques | Monitor schedules | Models | Best Results | References |
|---|---|---|---|---|---|---|---|---|---|---|
| | | | | | 922, 925, 958, 960 nm | | | | | |
| Potato and sweet potato tubers | DMC, SC | LTB | Temp.: 80 °C | 897-1753 nm | 1028, 1068, 1135, 1208, 1262, 1460 nm | NIR-HSI | 0, 40, 80, 120, 190, 260 min | FMCIA- $E_S$- RC-MLR (DMC), FMCIA -$E_S$-RC-PLSR (SC) | $R^2_p$ = 0.962 (DMC), $R^2_p$ = 0.963 (SC) RMSEP = 0.025 (DMC), RMSEP = 0.023 (SC) | Su and Sun (2017) |
| Tubers | VTC, TCD | LTB | Temp.: 80 °C | 900-1700 nm | 991, 1031, 1071, 1138, 1252, 1403, 1460, 1641 nm | NIR-HSI | 40, 80, 120, 190, 260 min | FMCIA-TBPANN | $R^2$p = 0.956 (VTC), $R^2$p = 0.992 (TCD) RMSEP = 0.012 (VTC) RMSEP = 0.145 (TCD) | Su and Sun (2016) |
| Cured meats | TVB-N | AD | Temp.: 52-58 °C | 400-1000 nm | 553, 583, 607, 643, 675, 709, 746, 908, 937 nm | VNIR-HSI | 0, 0.5, 1, 1.5, 2, 3, 4, 6, 8, 12, 16, 24, 32, 48 h | RC-MLR | $R^2_p$ = 0.861 RMSEP = 4.73 | Yang, Sun, and Cheng (2017) |
| Brine solutions | Inorganic constituents, alkalinity, phosphate | Natural Dehydration | – | 1000-2500 nm 4000-600 $cm^{-1}$ | – | NIRS, MIRS | once per week | PLSR | $R^2_p$ > 0. 90 ($Mg^{2+}$, $K^+$, $HCO_3^-$, $SO_4^{2-}$) (NIR) $R^2$ = 0.85 ($H_2PO_4^-$) (MIR) | Galvis-Sánchez et al. (2013) |
| Dry-cured ham | NaCl content | AD | Temp.: 4, 12-14, 16-18, 18-20 °C RH: 60%-70% | 833-2500 nm | – | FT-NIRS | 4, 7, 11, 15, 19, 22, 26, 30, 36 weeks | PLSR | $R^2$ = 0.91 RMSEV = 1.13 RPD = 3.33 | Collell et al. (2011) |
| Dry-cured meat | TBARS | AD | Temp.: 45, 50 °C | 400-1000 nm | – | VNIR-HSI | 0, 3, 5, 10, 15, 20, 25 h | PLSR | $R^2_p$ = 0.77 RMSEP = 0.97 | Aheto et al. (2020) |
| Fermented sausages | NaCl content | AD | Temp.: 12, 14, 16 °C RH: 80, 65, 72, 78.5, 90.8 % | 830-2500, 920-1800, 1100-2300 nm | – | FT-NIRS, NIRS, AOTF-NIRS | set 1: 0, 2, 4, 7, 9, 11, 14, 16, 18 days. set 2: 0, 2, 4, 7, 9, 11, 14, 16, 18, 21, 23, 25, 28, 30, 32, 35, 37, 39 days set 3: 0, 2, 5, 10, 20, 25, 35, 51, 68 days | PLSR | $R^2_p$ = 0.910 RMSEP = 0.220% | Collell et al. (2012) |
| Intact macadamia nuts | PV, AI | AD | Temp.: 30, 40, 60 °C | 866-2530 nm | – | NIRS | 0, 4, 6, 7 days | PLS | $R^2_C$ = 0.57 (PV) $R^2_C$ = 0.56 (AI) RMSEP = 0.6 (PV) RMSEP = 0.3 (AI) SEP = 0.55 meq/kg (PV) SEP = 0.29% (AI) | Carvalho, Leite, et al. (2019) |
| Organic apple wedges | SSC | HAD | Temp.: 60 °C | 1100-2300 nm | 1310 and 1878 nm | portable AOTF-NIRS | 0, 1, 2, 3, 4, 5, 6, 7, 8 h | iPLS | $R^2_p$ = 0.97 RMSEP = 4.63 | Moscetti, Raponi, et al. (2018) |
| Organic carrot slices | Carotenoids, SSC | HAD | Temp.: 40 °C | 1100-2300 nm | Carotenoids: 1100, 1394, 1754, 1900, 2038, 2236 nm | AOTF-NIRS | 0, 1, 2, 3, 4, 5, 6, 7, 8 h | iPLS | $R^2_p$ = 0.96 (Cariteniods) $R^2_p$ = 0.89 (SSC) RMSEP = 22.62 | Moscetti et al. (2017) |

| | | | | | | | | | | |
|---|---|---|---|---|---|---|---|---|---|---|
| | | | | | SSC: 1116, 1278, 1376, 1378, 2098, 2118 nm | | | | (Cariteniods) RMSEP = 4.19 (SSC) | |
| ODP | Total soluble solids, Sucrose, glucos, fructose | HAD | Temp.: 60 °C | 800-2400 nm | TSS: 910-1174, 1446-1938, 2048-2348 nm Sucrose: 904-1122, 1428-1790, 1972-2104 nm Glucose: 856-1060, 1340-1788 nm Fructose: 880-1058, 1410-1768 nm | NIRS | 2, 4, 6, 8, 10, 12 h | SCMWPLSR | $R^2_p$ = 0.990 (TSS) $R^2_p$ = 0.988 (the sucrose) $R^2_p$ = 0.984 (glucose) $R^2_p$ = 0.981 (fructose) RMSEP = 0.58 °Brix (TSS) RMSEP = 14.44 g/100 g (the sucrose) RMSEP = 6.72 g/100 g (glucose) RMSEP = 4.89 g/100 g (fructose) | Rongtong et al. (2018) |
| Pork sausages | NaCl | AD | Temp.: 12 °C Air velocity: 0.5 m/s RH: 58.6%-90.8% | 833-2500 nm | – | FT-NIRS | twice during fermentation, seven times during drying | PLSR | $R^2_p$ = 0.974 RMSEP = 0.116 | Collell et al. (2010) |
| Sweet potato | Carotenoids | HAD MD | Temp. (HAD): 85 °C Power (MD): 820 W Rotation rate (MD): 25 r/min | 250-2000 $cm^{-1}$ | 900 and 1600 $cm^{-1}$ | Raman | HAD: 15, 45, 75, 125 min MD: 3, 6, 8 min | PCA, PLS | $R^2$ = 0.96 (hot air) $R^2$ = 0.99 (microwave) RMSE = 16.28 g/100g (hot air) RMSE = 11.27 g/100g (microwave) | Sebben et al. (2018) |
| Falso guarana | Carotenoids, Classification | HAD | Temp.: 65, 85 °C Air velocity: 2 m/s | 400-2000 $cm^{-1}$ | 1006, 1157 or 1520 $cm^{-1}$ | Raman | 10, 20, 30, 100, 220, 280, 400 min | PCA, PLS | $R^2_p$ = 0.83 (85 °C) $R^2_p$ = 0.72 (85 °C/$TiO_2$) $R^2_p$ = 0.76 (65 °C/$TiO_2$) RMSEP = 25.98 (85 °C) RMSEP = 24.71 (85 °C/$TiO_2$) RMSEP = 24.72 (65 °C/$TiO_2$) | Carvalho, Sebben, et al. (2019) |

Abbreviations: AD = air drying; AI = acidity index; ANN = artificial neural network; AOTF = acoustic optic tunable filter; ATR = attenuated total reflectance; $a_w$ = water activity; B-D = brined-dehydrated; BFWA = binary fire-work algorithm; BPANN = back propagation artificial neural network; BPNN = back propagation neural network; $\Delta C$ = the absolute error; CAD = cold air dehydration; CARS = competitive adaptive reweighted sampling; CCR = correct classification rate; CUHAD = contact ultrasound assisted hot air drying; DMC = dry matter concentration; EMCVS = ensemble Monte Carlo variable selection; FIR = Far Infrared; FD = freeze-drying; FMCIA = first-derivative and mean centering iteration algorithm; FT = Fourier transform; FWC = freezable water content; H-D = heated-dehydrated; HAD = hot air drying; HSI = hyperspectral imaging; iPLS-DA = interval PLS-DA; iPLS = interval PLS regression; K-NN = K-nearest neighbor; LDA = linear discriminant analysis; LS-SVM = least-square support vector machines; LTB = low temperature baking; LWPLSR = locally weighted partial least square regression; MC = moisture content; MCU = moisture content uniformity; MCUVE = Monte-Carlo uninformative variable elimination; MD/MWD = microwave drying; MLR = multiple linear regression; MSI = multispectroscopy imaging; MVD = microwave vacuum drying; NIR-HSI = near-infrared hyperspectral imaging; NIR = near-infrared; NIRS = near-infrared spectroscopy; NRW = Nicholson-Ross-Weir; ODP = osmotically dehydrated papaya; PCA = principal components analysis; PFSP = purple fleshed sweet potato; PLS-DA = partial least square-discriminant analysis; PLS = partial least squares; PLSR = partial least squares regression; PS-MFD = pulse-spouted microwave freeze drying; PSMVD = microwave-assisted pulse-spouted bed vacuum-drying; PV = peroxide value; $R^2$ = coefficient of determination; RC = regression coefficients; RCV = regression coefficient vector; RPD = residual predictive deviation; RMSE = root mean square error; RV = regression vector; SC = starch concentration; SCMWPLSR = searching combination moving window partial least squares regression; SPA = successive projections algorithm; SSC = soluble solids content; SVM = support vector machine; SVMR = support vector machine regression; SWIR = shortwave infrared; TBARS = thiobarbituric acid reactive substances; TBPANN = three-layer back propagation artificial neural network; TCD = tuber cooking degree; TDS = time-domain spectroscopy; Temp.= temperature; TS = time series; UCS = ultimate compressive strength; VFD = vacuum freezing drying; VIP = variable importance in projection; Vis = visible wavelength; VNIR = visible near-infrared; VNIRS = visible near-infrared spectroscopy; VTC = volatility of tuber compositions; WBSF = Warner-Bratzler shear force.

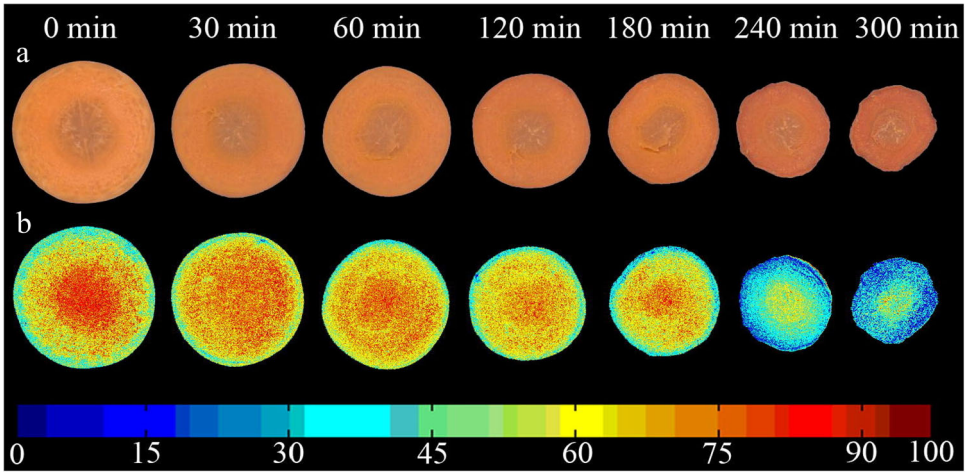


**Figure 2.** (a) RGB images and (b) TS-HSI visualization results of moisture contents of carrot slices during hot air drying (Liu et al. 2016).

vibrational spectral technologies, THz spectral techniques are still in the early development stage. Since the vibration frequency of hydrogen bonds are located in the THz region, the THz wave shows much higher absorption coefficients to MC than other food components. For instance, a typical absorbance value for water in food wafers is about 250 $cm^{-1}$, which is 16, 40 and 125 times higher than lipids, starch and protein, respectively (Afsah-Hejri et al. 2019; Parasoglou et al. 2010; Qin, Ying, and Xie 2013). Such a difference between MC and other components reduces the interferences from other components and enhances MC assessment accuracy, although the appearance of water could affect chemical analyses of THz spectra. In addition, compared with IR radiation, the stronger penetration ability of THz waves can improve the MC prediction accuracy for thick dehydrated samples, and the low power of THz sources does not significantly increase the temperature of samples (Zahid et al. 2019; Qin, Ying, and Xie 2013). Besides, combined with spectral imaging techniques, physicochemical visualization and spatial analyses during dehydration could be feasible under THz-TDS imaging techniques.

### *Spectral imaging techniques*

Most foods are heterogeneous in nature, limiting the assessment accuracy of point-based spectroscopic analyses. However, spectral imaging techniques combining spectroscopy and imaging techniques have been widely studied in agriculture and food science for more than 20 years (Lu and Chen 1999; Lu and Park 2015). Spectral imaging techniques provide both spectral and spatial information, making them powerful for dynamic visualization, evaluation and monitor of food physicochemical changes during dehydration (Wu, Wang, et al. 2012; Nguyen-Do-Trong, Dusabumuremyi, and Saeys 2018). Especially time-series hyperspectral imaging (TS-HSI), defined as a stack of hyperspectral images for the same sample acquired at various process times, is widely applied in assessing sample physicochemical changes during dehydration (Gowen et al. 2011; Xu, Gowen, and Sun 2018). As an example, Figure 2 shows the TS-HSI visualization results of MC and RGB images of carrot slices during hot air drying. Compared with the RGB images, HSI could visualize the dynamic change of MC concentration and distribution during dehydration. According to the volume of the spectral cube, spectral imaging techniques can be divided into multispectral imaging (MSI), HSI, and ultraspectral imaging (USI) (Feng and Sun 2012; Wu and Sun 2013a). Multispectral images contain far fewer wavelengths than hyperspectral images, leading to a faster scanning speed, less memory space requirement and chemometric calculation burden, and the cost of HSI for industrial application is expensive, especially for the small and medium-sized enterprise. Therefore, MSI systems would be a better choice for industrial applications (Ma, Sun, and Pu 2016). Currently, point-scanning (whiskbroom), line-scanning (push-broom), area-scanning (wavelength-scanning), and single-shot (Ma et al., 2019a; and 2019b; Wu and Sun 2013a) are four major strategies for spectral imaging acquisition. A typical schematic diagram of a push-broom scanning device is shown in Figure 3. The conveyor belt system in food manufacturers could replace the parts of the translation belt, sample holder and motor in Figure 3 to boost sensing efficiency, making such systems suitable for online industrial use (Lei, Lin, and Sun 2019). Besides, single-shot spectral imaging is the fastest method for making spectral video function possible, although such devices are still under development because their spectral and spatial resolutions are hard to meet the demands of food analyses yet (Ma et al. 2019b).

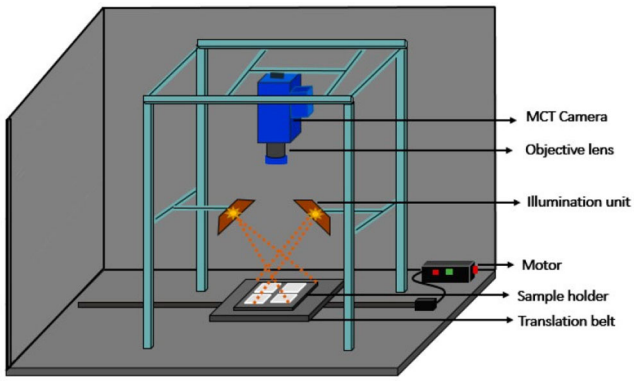


**Figure 3.** Typical schematic diagram of the push-broom hyperspectral imaging set up (Lee et al. 2020) (MCT = mercury-cadmium-telluride).

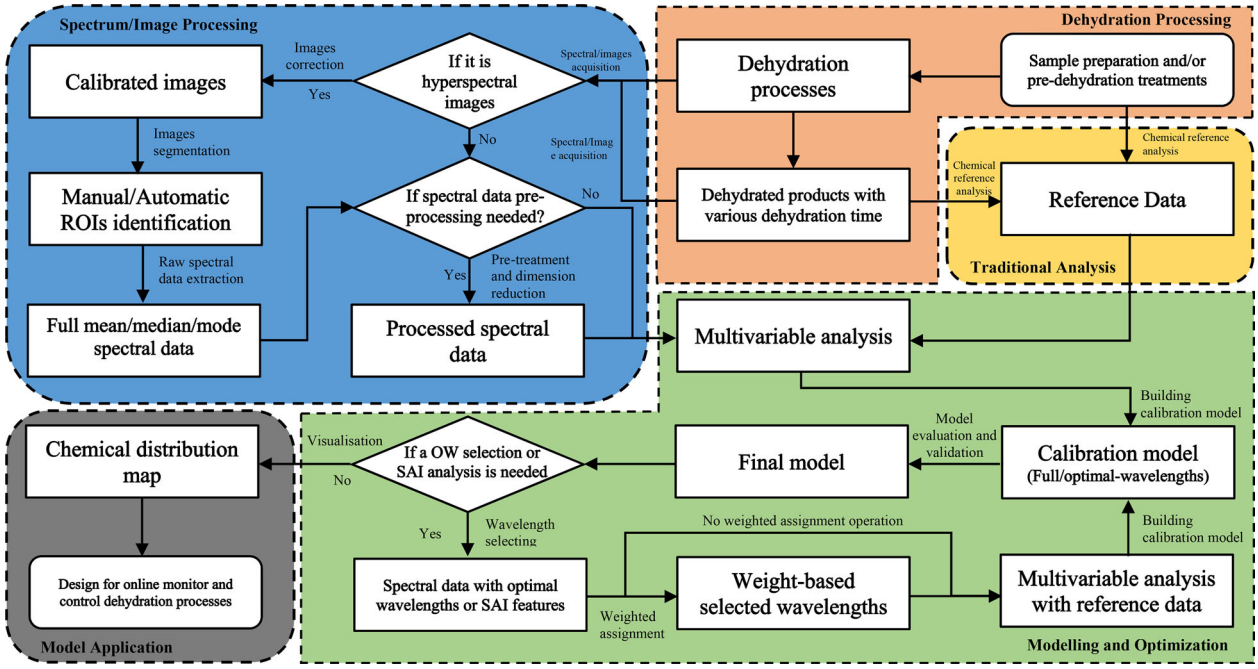


**Figure 4.** Typical steps to establish a vibrational spectral analysis model for online monitor and control of a food dehydration process (SAI = spectral absorption index; OW = optimal wavelength; ROIs = regions of interest).

### *Spectral data processing*

Spectral data processing correlates reference values with sample spectra to achieve a dynamic assessment of physico-chemical attributes during food dehydration. Figure 4 shows the typical procedure for establishing dehydration evaluation models.

### *Extraction and preprocessing of spectra*

Spectral data extraction aims to isolate regions of interest (ROIs) from the background and then extract the representative information from ROIs, followed by data preprocessing where the spectral quality is improved for model developments (Xie et al., 2015). Automatic segmentation of ROIs is much more rapid and suitable for industrial applications than manual segmentation, with no noticeable difference in accuracy (Wu, Shi, et al. 2012). In TS-HSI, physical appearance and spatial resolution vary in each image, Xu, Gowen, and Sun (2018) solved the problem using a geometric transformation algorithm to align the moving images with fixed images based on three white paper pieces stuck on the sidewall of the Petri dish. Besides, although the mean spectra of ROIs are most commonly adopted, Ma, Qu, and Sun (2017) showed that mean and median spectra were more suitable than mode spectra, and they also compared the mean and median spectra and showed that the integrated median wavelengths group was the optimum spectral profiles (Ma et al. 2017). Moreover, Huang et al. (2014) attempted to use image entropy parameters to replace or combine mean reflectance data, although it did not show apparent improvements in prediction accuracy.

Spectral preprocessing algorithms aim to improve spectral quality by reducing interference noise, including instrumental drift, light scattering and environment noise. These methods can be divided into scatter-correlation and spectral derivatives. Standard normal variate (SNV), multiplicative scatter correction (MSC), and normalization are popular algorithms of the former, while the latter include Savitzky-Golay (SG) smooth, moving average smooth, first and second derivatives and Norris-Williams (NW) derivatives (Lin and Sun 2020a; Liu et al. 2018; Lohumi et al. 2015). These preprocessing methods can also be classified into sample-based and variable-based approaches. The effect of the former on an individual sample is independent of other samples in the dataset, while the latter numerically prepare variance data for modeling. Therefore, the former should have the priority for application compared with the latter (Pu and Sun 2016; Wise et al. 2006).

### *Model developments*

Multivariate analyses and effective wavelengths selection methods are essential for correlating experimental reference values with spectra to develop dehydration assessment models (Cheng et al., 2018). Effective wavelengths, carrying the most critical information relevant to target substances, are more efficient than full wavelengths for modeling because spectral data are not enormous but high collinear (Lei and Sun 2020; Lin and Sun 2020a; Ma et al., 2018; Qu et al. 2017; Wu, Wang, et al. 2012). Regression coefficients (RC) of partial least square (PLS) (Cheng et al., 2016a) models are the most adopted wavelength selection methods for food dehydration evaluation models. Other algorithms, containing successive projection algorithms (SPA), competitive adaptive reweighted sampling (CARS), and Monte-Carlo uninformative variable elimination (MCUVE), are widely used in food dehydration evaluation. Besides, novel wavelength selection methods, including first-derivative and mean centering iteration algorithm (FMCIA) (Su and Sun 2016, 2017), binary

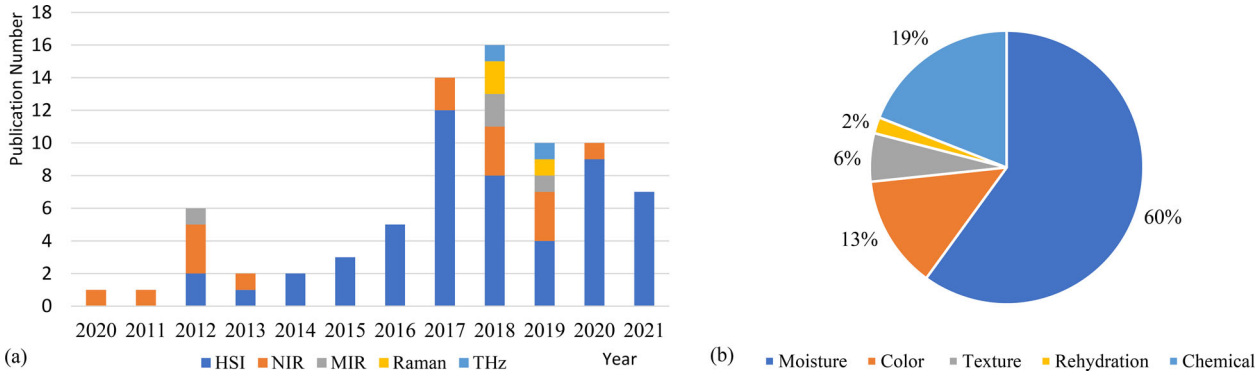


**Figure 5.** Research publications of (a) vibrational spectral techniques coupled with chemometrics for the evaluation of dehydration processes since 2010 and (b) percentage of each quality attribute in these studies.

firework algorithm (BFWA) (Yu et al. 2019), and variable importance in projection (VIP) (Lee et al. 2020), have been proven to be more efficient in wavelengths selection. Additionally, a manual wavelength reducing strategy could be found in the research by Amjad et al. (2018), in which models based on this method had broader applicability for different samples. In addition, critical wavelengths can be weighted to improve the accuracy of the partial least squares regression (PLSR) model (Qu et al. 2017). Furthermore, the morphological feature of mean spectral curves refined by spectral absorption index (SAI) showed the potential to replace optimal wavelengths for model development, although the dehydration evaluation accuracy of such a model was not as good as the optimal wavelength based model (Ma, Sun, and Pu 2016).

Multivariate regression algorithms correlate target attributes with spectra. For dehydration evaluation, both linear regression methods, including multiple linear regression (MLR), PLSR, and least squares support vector machines (LS-SVMs) (Dai et al., 2016), and non-linear regression techniques, such as artificial neural networks (ANN) have been used. Although non-linear prediction models generally have more robust and accurate performances than liner methods (Mohammadi-Moghaddam et al. 2018; Su, Bakalis, and Sun 2019a; Su, Bakalis, and Sun 2019b; Özdoğan et al., 2021), PLSR is the most widely used algorithm in food dehydration assessment, which can be calculated as (Liu, Sun, and Zeng 2014):

$$X = TP^T + E \quad (1)$$

$$y = Tq^T + f \quad (2)$$

$$W^* = W(P^T W)^{-1} \quad (3)$$

$$T = XW^* \quad (4)$$

$$\beta = W^* q^T = W(P^T W)^{-1} q^T \quad (5)$$

$$\hat{y} = XW_k B = TB \quad (6)$$

where $X$ refers to the spectral matrix with $n \times m$ dimension ($n$ and $m$ are the samples number and wavelengths number, respectively), $T$ is the wavelength scores, $P$ is the $m \times k$ matrix of $X$ loading and $q$ is the response data ($n \times c$) that need to be predicted from $X$, where $c$ refers to the number of response variables. $E$ and $f$ stand for random errors in $X$ and $y$, respectively, while $W$ is the PLS weights, and $W^*$ is the $m \times k$ matrix of $X$ weights, $B$ is the matrix that contains the regression coefficients ($m \times c$) and $\hat{y}$ is the predicted value of quality attributes.

Since MLR can only deal with variables less than samples number, wavelength selection is necessary for MLR model development (Kamruzzaman, Makino, and Oshita 2016; Sun et al. 2017). In addition, few studies focused on developing models for classifying process stages and dehydration methods, with overall correct classification rates (CCR) being between 76.923%-100% (Gonzalez-Mohino et al. 2020; Lin, Xu, and Sun 2021; Moscetti et al. 2017; Moscetti, Raponi, et al. 2018; Xie et al. 2013; 2014).

### *Model evaluation*

To evaluate the performance of dehydration assessment models, the coefficient of determination ($R^2$), root mean square error (RMSE) and the ratio of the standard error of prediction to deviation (RPD) are commonly calculated (Pan et al., 2018). Relatively high $R^2$ ($> 0.8$) and RPD ($> 3$), and low RMSE indicate good performance of models (Rongtong et al. 2018; Wokadala et al. 2020; Yang, Sun, and Cheng 2017). Also, the details of Fisher's $F$-test have been adopted to evaluate statistical differences between models, and other robustness indicators of models such as bias control limit (BCL) and unexpected error control limit (UCL) have also been employed for model evaluation (Moscetti, Sturm, et al. 2018).

## Dynamic assessment and control of food dehydration

Figure 5 shows the number of publications since 2010 on vibrational spectral techniques coupled with chemometric for evaluating dehydration processes and on assessing quality attributes. The total publication number of relevant research summarized from publication databases of Google Scholar, Web of Science and Scopus has obviously increased in the past decade. In these techniques, HSI occupies the largest proportion for quality evaluation, followed by NIRS, while the research related to MIRS and Raman spectroscopy emerges in recent years with relatively low frequency, and

few studies have employed THz-TDS coupled with chemometrics for the food dehydration assessment.

### Moisture contents

MC affects microorganism growth, fat oxidation, and enzyme activity of food. Removing most MC from food is the ultimate purpose of dehydration. Traditional methods for MC determination, such as the thermo-gravimetric method, oven-dry method and Karl Fisher titration, are time-consuming and destructive, which are not suitable for continuous measurement (Pu and Sun 2015; Qu et al. 2017; Sun et al. 2017). Therefore, vibrational spectral techniques in tandem with chemometrics have been developed for dynamic analysis of food dehydration.

### Prediction of moisture contents

By combining spectral data with spatial image, spectral imaging techniques dominate the research of evaluating MC during food dehydration in the past decade, while few studies using MIRS, Raman spectral analysis, and THz-TDS to monitor MC. For dehydration techniques, hot air drying gained the most intensive research in the past decade, followed by microwave-based drying (Table 2). Other dehydration techniques include freeze-drying (Kauppinen et al. 2013; Ma, Qu, and Sun 2017; Qu et al. 2017), solar drying (Wokadala et al. 2020), PSMVD (Huang et al. 2014; Huang et al. 2015; Yu et al. 2019), brined dehydration (Ma, Sun, and Pu 2016), natural dehydration (Xu, Gowen, and Sun 2018), and heated-dehydration (Ma, Sun, and Pu 2017; Ma, Sun, and Pu 2016).

From Table 2, the average $R^2$ of NIRS models for MC and $a_w$ prediction are 0.934 and 0.905, respectively, while the average $R^2$ of spectral imaging MC prediction models is 0.959, indicating that spectral imaging has better MC evaluation accuracy than NIRS. The reason is that point-based spectroscopic techniques can not satisfactorily be used for evaluating the inhomogeneous MC distribution. Among the studies listed in Table 2, Czaja et al. (2018) compared the MC prediction accuracies during pasta dehydration using NIRS, MIRS and Raman spectroscopy, showing that NIRS and MIRS were more accurate than Raman spectroscopy. Su, Bakalis, and Sun (2019b) showed that NIR-HSI could predict MC better than MIR-HSI during microwave drying although both infrared spectral imaging techniques provided satisfactory results.

The main barrier for spectroscopic techniques is their point-based feature, while food is heterogeneous in nature. Therefore, multi-points scanning (Collell et al. 2011) and multi-sensors detection (Kauppinen et al. 2013) using NIRS have been developed. Kauppinen et al. (2013) successfully used three NIRS probes integrated with a freeze-dryer to predict the non-uniform sublimation rates and the endpoint of dehydration. Moreover, vibrational spectral techniques have successfully been used to assess other MC related attributes during food dehydration, including water status (Younas et al. 2020), water fractions (Younas, Mao, Liu, Liu, et al. 2021; Younas, Mao, Liu, Murtaza, et al. 2021), freezable water content (Sun et al. 2017) and moisture content uniformity (MCU) (Huang et al. 2015), and phase classification (Gonzalez-Mohino et al. 2020; Moscetti et al. 2017; Moscetti, Raponi, et al. 2018).

The dynamic distribution of MC due to dehydration also attracts much research interest. It has been shown that various dehydration patterns can be successfully observed by using spectral imaging techniques. The MC at the edges of food samples normally drops faster than that of center parts during convective drying (Lin, Xu, and Sun 2016, 2020b; Sun et al. 2020; Wu, Wang, et al. 2012) as the edge surface has more contact with hot air, leading to a higher moisture evaporation rate. However, using MC distribution maps generated by HSI techniques, Pu and Sun (2015, 2016) and Lin, Xu, and Sun (2020a, 2020b) showed that in microwave-based dehydration, the MC distribution patterns in food samples are the opposite, i.e., MC from center parts of food samples is generally reduced faster than the edges due to the non-uniform microwave heating dissipation, in which the heat energy in the center of food samples might be more difficult to dissipate, giving a higher temperature in the center and thus the moisture evaporation rate was higher, resulting in a higher drop in moisture content, although Liu et al. (2018) reported that MC at the center was higher than that at the edges of beef slices in the final stage of microwave drying (MD) by using HSI visualization.

### Process optimization

Based on the MC distribution maps generated by HSI techniques, dehydration processes can be optimized to produce even and uniform MC distribution in the dried products, thus leading to high-quality products. Using HSI, Pu and Sun (2017) found that the combination of hot air drying (HAD) and MVD could improve dehydration efficiency, MC uniformity, and product quality for mangos as compared with individual HAD and MVD. Lee et al. (2020) reported similar results in combining HAD with MD to dry radish slabs. Besides, HSI was used to compare the dehydration patterns of gingers, mangoes and potatoes with different slicing shapes (Amjad et al. 2018; Lin, Xu, and Sun 2020; Lin and Sun 2020b; Moscetti, Sturm, et al. 2018; Pu and Sun 2016, 2017), showing that the cutting direction, geometry and thickness of slices influenced the dehydration rate, MC distribution and products quality. Moreover, Xu, Gowen, and Sun (2018) reported that adding a higher concentration of plasticizer helped form a more robust hydrogen bond network in dehydrated edible films as observed by TS-HSI.

On the other hand, effects of sample treatments such as bleaching, water immersion, acid processing, maturation, freezing, thawing, seasoning, brining, vacuum and ultrasound treatments on dehydration behavior and products quality have also been successfully evaluated by HSI with acceptable accuracy (Achata et al. 2021; Crichton et al. 2018; Netto et al. 2021; Retz et al. 2017; von Gersdorff et al. 2018). In addition, using NIRS, different dehydration patterns and model performances of blenched and microwave

pretreated apple wedges and carrot slices were also investigated (Moscetti et al. 2017, Moscetti, Raponi, et al. 2018). Crichton et al. (2018) showed that although pretreatments affected the dehydration efficiency, the optimal wavelengths selected for model developments remained stable across various pretreated samples.

## Physical quality attributes

Physical quality attributes including chromaticity, texture and rehydration ability can undergo significant changes during dehydration, and therefore the evaluation of these attributes during the process is essential for product quality control.

### Chromaticity

Chromaticity is a critical quality attribute of food that decides the first impression of customers as it reflects the freshness and some chemicals contents of the food product such as chlorophyll, carotene, myohemoglobin (Devahastin and Niamnuy 2010). However, a series of physicochemical reactions, such as Maillard reaction, oxidation, reduction and caramelization, could change the color of products, which might lead to identical chromaticity of dehydrated products. Therefore, chromaticity is not suitable to be used as the single quality indicator for both dehydration processes and dehydrated food (Moscetti, Raponi, et al. 2018; Retz et al. 2017).

Traditional color measurements are mainly based on colourimeter measurements, which is in direct contact with food surface and could cause contamination. On the other hand, HSI and NIRS, using wavelengths mainly in the VNIR region, have been developed to predict the CIELAB color parameters of food in a fast and nondestructive way with $R^2$ values ranging from 0.53 to 0.99 (Table 2), with the CIELAB parameters of a* and b* being most widely adopted to evaluate color changes during dehydration with $R^2$ from 0.53 to 0.99 for a* and 0.73 to 0.98 for b*. Furthermore, Retz et al. (2017) used VNIR-HSI and NIRS to successfully evaluate CIELAB parameter L* during dehydration and achieved the best prediction results with $R^2 = 0.96$ and RMSEP = 1.09 based on the CARS-PLSR model. In addition, von Gersdorff et al. (2021) established a model valid for MC and CIELAB L*, a*, b* measurements of beef slices. Besides, other CIELAB parameters such as $h^*$ (Moscetti et al. 2017; Moscetti, Sturm, et al. 2018), $C^*$ (Moscetti, Raponi, et al. 2018) and $\Delta E$ (Huang et al. 2014) have also been used in HSI and NIRS evaluation of dehydration processes.

Similar to MC prediction models, certain dehydration pretreatments on samples could influence the color prediction model development. von Gersdorff et al. (2018) showed that optimal wavelengths changed with different sample preparation methods for drying beef slices, but Crichton et al. (2018) reported that the optimal wavelengths for evaluating the color changes of apple slices remained unchanged with various pretreatments. Such a disagreement could be due to the different preparations of beef samples, which resulted in a different extent of conversion from red oxymyoglobin to brown metmyoglobin pigment, varying the initial chromaticities and changing pattern of the samples. However, the initial color of apples did not change by the pretreatments, and the phenolic compounds were protected from enzymatic browning.

### Texture

Texture features play important roles in determining the quality and value of dehydrated foods. Texture changes are related to MC, chemical components, and structure variation of food due to dehydration, which is affected by dehydration parameters, such as temperature, air velocity and time. Traditional methods in determining texture include the three-point bending test, Warner-Bratzler shear force (WBSF) test, Magness-Taylor (MT) puncture test, and compression test, which are mainly based on the precise response to compression, puncture, shear stress, impact or creep. These methods are inefficient, sample-destructive and not suitable for dynamic online process monitoring. Therefore vibrational spectral imaging mainly including HSI and Fourier-transform mid-infrared (FT-MIR) microspectral imaging has been investigated for texture analyses. While NIRS has been proven for its ability to accurately predict food texture (Sirisomboon et al. 2012; Yancey et al. 2010), applications of other vibrational spectroscopies have rarely been reported in the past decade.

For HSI, Ma et al. (2017) established a PLSR model based on ten critical wavelengths to simultaneously predict four texture parameters of grass carp fillets during vacuum freeze-drying with $R^2_p$ between 0.7982 and 0.8774. Mohammadi-Moghaddam et al. (2018) achieved high accuracy in using an ANN model based on full wavelengths to predict four texture parameters of pistachio kernels under air-drying as affected by various drying temperatures and air velocities, with $R^2_p$ and RMSEP of prediction models being between 0.876-0.957 and 2.366-15.757 N, respectively. Besides, Pu et al. (2018) established a support vector machine regression (SVMR) model based on full wavelengths and achieved high prediction accuracy with $R^2_p$ of 0.927 and 0.961 for hardness and fracturability, respectively. For FT-MIR microspectral imaging, Su, Bakalis, and Sun (2018) established an FMCI-SPA-LWPLSR model for tuber textural property (TTP) evaluation during microwave drying. Based on the three combinations of 6 critical wavelengths in the mid-infrared region, a mean $R_p$ of 0.709 for six TTP features was achieved. As penetration of VNIR-HSI is shallow and structure changes at the end of dehydration happen close to the core of samples, food texture evaluation at the end stage of dehydration is not accurate as early and middle stages, reducing the overall texture evaluation accuracy of HSI (Nguyen-Do-Trong, Dusabumuremyi, and Saeys 2018). With stronger penetration ability (Afsah-Hejri et al. 2019), THz-TDS imaging might achieve more accurate texture evaluation than VNIR spectral imaging, especially at the end stage of dehydration.

### Rehydrating property

The rehydrating property of dried food products is an important indicator of high-quality drying processes, as dried foods from optimum drying conditions possess more rapid and complete rehydration ability than poorly dried products (Fellows 2009), and traditional evaluations of rehydrating property are based on comparing the weight difference between dried and rehydrated samples. Vibrational spectral imaging techniques have been used to predict the rehydrating ability of dehydrated foods as affected by different dehydration times. Ma, Qu, and Sun (2017) visualized the rehydration mass gain percentages of grass carp flakes during vacuum freezing drying by using a VNIR-HSI. Nine critical wavelengths were selected by RC developing the PLSR model, achieving an $R^2_p$ and RMSEP of 0.8278 and 9.79%, respectively. A higher $R^2_p$ of 0.957 was obtained by Lin and Sun (2020b), who used a NIR-HSI to monitor the rehydration rates of ginger slices based on the PLSR prediction model developed using full wavelengths. Although HSI has been proven for its ability to monitor the rehydration ability of foods, relevant research is still insufficient. Future studies could attempt to use spectral imaging to evaluate the rehydration property of samples under more dehydration conditions and compare distribution patterns of this property among different dehydration methods for product quality enhancement.

## Chemical components

Chemical components change during dehydration, especially for heat-sensitive foods. Traditional chemical component analysis methods such as high-performance liquid chromatography (HPLC) are based on sample pretreatment and analytical chemistry (Liu et al. 2018; Liu et al. 2017; Cheng et al., 2016b; Sturm et al. 2020). The pretreatments aim to eliminate interferences from other components, which are time-consuming and destructive (Ma and Sun, 2020; Cheng et al., 2017).

MIR spectral techniques with fingerprint features show strong ability in chemical component analyses and a large number of studies are available on analyzing the change of molecular structure for samples during dehydration (Chranioti, Chanioti, and Tzia 2016; Elavarasan et al. 2016; Fan, Xiang, and Zhao 2021), but only a few studies apply chemometric models to quantify or classify chemical contents. Besides, due to the strong absorption of water, THz spectral techniques might only have the potential to analyze chemical contents at the final stage of food dehydration, although no relevant studies have been published yet. In addition, spectral imaging, NIRS, and Raman spectral techniques have been combined with chemometrics to evaluate chemical attribute changes of samples during dehydration.

### Carbohydrates

Carbohydrate contents, such as sucrose, glucose, fructose, and starch, can be evaluated by NIRS and spectral imaging techniques as affected by convective drying. Rongtong et al. (2018) used NIRS to evaluate sucrose, glucose and fructose of osmotically dehydrated papaya prepared by five concentrations of sucrose during air-drying and achieved a high $R^2$ of over 0.98 for all three kinds of carbohydrates. Su and Sun (2017) monitored starch content (SC) and dry matter concentration (DMC) of tubers by using a NIR-HSI during low-temperature baking at 80 °C, and the PLSR and MLR models based on only six critical wavelengths selected by FMCIA and RC were used to predict SC and DMC, achieving an $R^2_p$ of 0.963 and 0.962, and RMSEP of 0.023 and 0.025, respectively.

### Inorganic salts

Dynamic changes of inorganic constituents including bound ion and free ion during dehydration were monitored by NIRS. In the studies conducted by Collell et al. (2011, 2012), various NIRS, including remote, on-contact and portable devices, were used for surface NaCl content evaluation of dry-cured ham and fermented sausages during convective drying. With FT-NIRS, the best $R^2$ of 0.91 and RPD of 3.3 were obtained in predicting the NaCl contents in both dry-cured ham and fermented sausages.

Galvis-Sánchez et al. (2013) employed NIRS and MIRS to evaluate the concentrations of alkalinity and phosphate in brine solutions for making sea salt and the final dried sea salt during natural drying. Interestingly, the NIRS showed better prediction ability for the brine evaluation, but both MIRS and NIRS showed low accuracy for the evaluation of dried salts. The reason could be the evaluation was mainly based on the detection of the perturbation of the hydrogen bonds between water and ions and the free ions in the solution did not absorb the IR wave.

### Quality deterioration indicators

Quality deterioration indicators of dried foods, including thiobarbituric acid reactive substances (TBARS), peroxide value (PV), acidity index (AI) and total volatile basic nitrogen (TVB-N) changes due to the high temperature of some dehydration processes. For evaluating the breakdown of the hydroperoxides, Aheto et al. (2020) used a VNIR-HSI to predict TBARS values of dry-cured pork belly during air drying, with $R^2_p = 0.77$. As analytical parameters of fat oxidation degree, PV and AI of intact macadamia nuts were monitored by NIRS during air drying (Carvalho, Leite, et al. 2019). Although the models established showed poor accuracy with $R^2_c$ of 0.57 and 0.56 and standard error for prediction (SEP) of 0.55 meq/kg and 0.29% for PV and AI, respectively, they were still useful since the SEP just accounted for 18% and 28% of the maximum quality limits for PV and AI, respectively. TVB-N reflects the existence of non-protein nitrogenous and toxic small-molecule compound, and Yang, Sun, and Cheng (2017) used VNIR-HSI to monitor the changes of this indicator during dehydration of cured meat, and the RC-MLR model developed based on nine selected wavelengths achieved an $R^2_p$ of 0.861 and RMSEP of 4.73, indicating the feasibility of using the model for visualizing the TVB-N dynamic distribution during drying.

### Other components

Other components can also be affected during dehydration, and vibrational spectral techniques have been studied to evaluate changes of volatile chemicals, anthocyanins, carotenoids and soluble solids content during food dehydration.

Sturm et al. (2020) employed VNIR-HSI to evaluate volatile substances, containing 1-octen-3-ol, $\beta$ -Ocimen and myrcene of hops during dehydration, and the MCUVE-PLS model established could predict the uniform changes of volatile substances in hops during dehydration, with $R^2_p$ between 0.83 and 0.64, while Su and Sun (2016) used NIR-HSI with the three-layer back propagation artificial neural network (TBPANN) model to predict the changes in the volatility of tuber compositions (VTC) and tuber cooking degree (TCD) during dehydration, realizing $R^2$ of 0.956 and 0.992, respectively.

Anthocyanin content in purple-fleshed sweet potato (PFSP) during dehydration was monitored by VNIR-HSI. The RC-MLR model based on ten selected wavelengths exhibited an acceptable accuracy with $R^2_p$ of 0.866 and RMSEP of 0.302 mg/g (Liu et al. 2017), while the CARS-PLSR model achieved $R^2_p$ of 0.847 and 0.859 for total anthocyanin evaluations of samples dried by hot-air drying and microwave drying, respectively (Tian, Aheto, Dai, et al. 2021). Besides the spectral imaging techniques, spectroscopic techniques have also been employed for evaluating other components during food dehydration. These applications include NIRS for soluble solids contents (SSC) with $R^2_p$ ranging from 0.89 to 0.99 (Moscetti et al. 2017; Moscetti, Raponi, et al. 2018; Rongtong et al. 2018), acoustic optic tunable filter NIRS for total carotenoid changes of carrot slices with $R^2$ of 0.96 (Rongtong et al. 2018), and Raman spectroscopy for carotenoid of sweet potato with $R^2_p$ between 0.96 and 0.99 (Sebben et al. 2018), but in the last case, the sweet potato samples were pretreated with $TiO_2$ before Raman spectral analysis, limiting its application for dynamic online monitoring. However, Carvalho, Sebben, et al. (2019) compared the prediction accuracy of carotenoids of falso guarana using Raman spectroscopy with and without pretreating the samples with $TiO_2$ during hot air drying, and showed that higher predictive accuracy ($R^2_p = 0.83$) was obtained for samples without pretreatment as compared with $R^2_p$ between 0.72 and 0.76 for those with pretreatment. Therefore, Raman spectral techniques without the need for sample pretreatments possess potentials for online application.

## Conclusions and future trends

Researchers have made great efforts in developing vibrational spectral analysis technologies in the food dehydration field during the past decade. The current review fills the gap that a comprehensive review lacks regarding applying the vibrational spectral technologies combined with chemometric in dynamically evaluating food dehydration processes. NIRS, MIRS, Raman spectroscopy, THz-TDS and spectral imaging, emerging as rapid and noninvasive tools, have been successfully applied to monitor critical attributes of food undergoing dehydration, including dynamic evaluation of MC, chromaticity, texture properties, rehydration ability, and chemical compounds.

MC evaluation occupies the largest percentage in these applications, while assessments of rehydration and texture attributes are relatively insufficient. Among all spectral techniques, spectral imaging, whose research frequency has increased obviously since 2012 and dominates relevant studies, exhibits the highest accuracy on MC dynamic evaluation and shows strong abilities in monitoring chromaticity, texture properties, rehydration ability and chemical components during food dehydration. Besides, NIRS is good at dynamic analyses of MC, color and chemical components during food drying, and MIRS is mainly used for analyzing MC, texture properties and chemical components. Moreover, Raman spectral technique is not suitable for MC evaluation due to the low sensitivity to water, but it exhibits great power for noninvasive dynamic monitoring chemical components during food dehydration. The THz spectral technique shows great MC monitoring potential although relevant applications are insufficient. For dynamic MC monitoring, NIRS shows lower prediction accuracy compared with HSI but has higher prediction ability than MIRS and Raman spectroscopy.

Future studies should compare the MC prediction accuracy between NIR-HSI and THz spectral techniques. In addition, the main barrier for spectroscopic techniques is their point-based feature that limits its widespread applications as food products are heterogeneous in nature, therefore further research should focus more on applications of the multi-point detection strategy and developing more novel and powerful chemometric models for embedding the vibrational spectral techniques into industrial drying set-ups. The application of vibration spectral analyses in monitoring textures and rehydration property of food during dehydration as well as nutritional attributes, in particular thermal sensitive contents, should also be further explored. Moreover, more efforts should be devoted to understanding the influence of real-time dehydration conditions on spectroscopic performance in future. Finally, as the application of THz spectral techniques is still at an early stage, more research should be focused on this area.

## Funding

Yuqiao Ren would like to acknowledge University College Dublin (UCD) and China Scholarship Council (CSC) for financial support to his PhD research under the UCD-CSC funding scheme.

## References

Achata, E. M., C. Esquerre, K. S. Ojha, B. K. Tiwari, and C. P. O'Donnell. 2021. Development of NIR-HSI and chemometrics process analytical technology for drying of beef jerky. *Innovative Food Science & Emerging Technologies* 69:102611. doi: 10.1016/j.ifset.2021.102611.

Afsah-Hejri, L., P. Hajeb, P. Ara, and R. J. Ehsani. 2019. A comprehensive review on food applications of Terahertz spectroscopy and

imaging. *Comprehensive Reviews in Food Science and Food Safety* 18 (5):1563–621. doi: 10.1111/1541-4337.12490.

Aheto, J. H., X. Y. Huang, X. Y. Tian, R. Q. Lv, C. X. Dai, E. Bonah, and X. H. Chang. 2020. Evaluation of lipid oxidation and volatile compounds of traditional dry-cured pork belly: The hyperspectral imaging and multi-gas-sensory approaches. *Journal of Food Process Engineering* 43 (1):e13092. doi: 10.1111/jfpe.13092.

Amjad, W., S. O. J. Crichton, A. Munir, O. Hensel, and B. Sturm. 2018. Hyperspectral imaging for the determination of potato slice moisture content and chromaticity during the convective hot air drying process. *Biosystems Engineering* 166:170–83. doi: 10.1016/j.biosystemseng.2017.12.001.

Bhatta, S., T. Stevanovic Janezic, and C. Ratti. 2020. Freeze-drying of plant-based foods. *Foods* 9 (1):87. doi: 10.3390/foods9010087.

Borovkova, M., M. Khodzitsky, P. Demchenko, O. Cherkasova, A. Popov, and I. Meglinski. 2018. Terahertz time-domain spectroscopy for non-invasive assessment of water content in biological samples. *Biomedical Optics Express* 9 (5):2266–76. doi: 10.1364/BOE.9.002266.

Braeuer, A. S., J. J. Schuster, M. T. Gebrekidan, L. Bahr, F. Michelino, A. Zambon, and S. Spilimbergo. 2017. In situ Raman analysis of $CO_2$-assisted drying of fruit-slices. *Foods* 6 (5):37. doi: 10.3390/foods6050037.

Carvalho, L. C., M. L. Leite, C. L. M. Morais, K. M. G. Lima, and G. H. A. Teixeira. 2019. Non-destructive assessment of the oxidative stability of intact macadamia nuts during the drying process by near-infrared spectroscopy. *LWT-Food Science and Technology* 103:101–7. doi: 10.1016/j.lwt.2018.12.056.

Carvalho, D. G., J. A. Sebben, N. F. de Moura, J. O. Trierweiler, and J. D. S. Espindola. 2019. Raman spectroscopy for monitoring carotenoids in processed Bunchosia glandulifera pulps. *Food Chemistry* 294:565–71. doi: 10.1016/j.foodchem.2019.04.120.

Chakravartula, S. S. N., C. Cevoli, F. Balestra, A. Fabbri, and M. Dalla Rosa. 2019. Evaluation of drying of edible coating on bread using NIR spectroscopy. *Journal of Food Engineering* 240:29–37. doi: 10.1016/j.jfoodeng.2018.07.009.

Chandrasekaran, S., S. Ramanathan, and T. Basak. 2013. Microwave food processing—A review. *Food Research International* 52 (1):243–61. doi: 10.1016/j.foodres.2013.02.033.

Cheng, W., D.-W. Sun, H. Pu, and Y. Liu. 2016a. Integration of spectral and textural data for enhancing hyperspectral prediction of K value in pork meat. *LWT- Food Science and Technology* 72:322–9. doi:10.1016/j.lwt.2016.05.003.

Cheng, W., D.-W. Sun, and J.-H. Cheng. 2016b. Pork biogenic amine index (BAI) determination based on chemometric analysis of hyperspectral imaging data. *LWT* 73:13–9. doi:10.1016/j.lwt.2016.05.031.

Cheng, W., D.-W. Sun, H. Pu, and Q. Wei. 2017. Chemical spoilage extent traceability of two kinds of processed pork meats using one multispectral system developed by hyperspectral imaging combined with effective variable selection methods. *Food Chemistry* 221:1989–96. doi:10.1016/j.foodchem.2016.11.093.

Cheng, W., D.-W. Sun, H. Pu, and Q. Wei. 2018. Heterospectral two-dimensional correlation analysis with near-infrared hyperspectral imaging for monitoring oxidative damage of pork myofibrils during frozen storage. *Food Chemistry* 248:119–27. doi:10.1016/j.foodchem.2017.12.050.

Cheng, W., K. M. Sørensen, R. J. Mongi, B. K. Ndabikunze, B. E. Chove, D.-W. Sun, and S. B. Engelsen. 2019. A comparative study of mango solar drying methods by visible and near-infrared spectroscopy coupled with ANOVA-simultaneous component analysis (ASCA). *LWT-Food Science and Technology* 112:108214. doi: 10.1016/j.lwt.2019.05.112.

Cho, J. S., J. Y. Choi, and K. D. Moon. 2020. Hyperspectral imaging technology for monitoring of moisture contents of dried persimmons during drying process. *Food Science and Biotechnology* 29 (10):1407–12. doi: 10.1007/s10068-020-00791-x.

Chranioti, C., S. Chanioti, and C. Tzia. 2016. Comparison of spray, freeze and oven drying as a means of reducing bitter aftertaste of steviol glycosides (derived from Stevia rebaudiana Bertoni plant)-Evaluation of the final products. *Food Chemistry* 190:1151–8. doi: 10.1016/j.foodchem.2015.06.083.

Collell, C., P. Gou, J. Arnau, and J. Comaposada. 2011. Non-destructive estimation of moisture, water activity and NaCl at ham surface during resting and drying using NIR spectroscopy. *Food Chemistry* 129 (2):601–7. doi: 10.1016/j.foodchem.2011.04.073.

Collell, C., P. Gou, J. Arnau, I. Munoz, and J. Comaposada. 2012. NIR technology for on-line determination of superficial a(w) and moisture content during the drying process of fermented sausages. *Food Chemistry* 135 (3):1750–5. doi: 10.1016/j.foodchem.2012.06.036.

Collell, C., P. Gou, P. Picouet, J. Arnau, and J. Comaposada. 2010. Feasibility of near-infrared spectroscopy to predict $a_w$ and moisture and NaCl contents of fermented pork sausages. *Meat Science* 85 (2):325–30. doi: 10.1016/j.meatsci.2010.01.022.

Craig, A. P., A. S. Franca, and J. Irudayaraj. 2013. Surface-enhanced Raman spectroscopy applied to food safety. *Annual Review of Food Science and Technology* 4:369–80. doi: 10.1146/annurev-food-022811-101227.

Craig, A. P., A. S. Franca, and J. Irudayaraj. 2015. Vibrational spectroscopy for food quality and safety screening. In *High throughput screening for food safety assessment*, ed. A. K. Bhunia, M. S. Kim, and C. R. Taitt, , 165–94. Cambridge, UK: Woodhead Publishing.

Crichton, S., B. Sturm, and A. Hurlbert. 2015. Moisture content measurement in dried apple produce through visible wavelength hyperspectral imaging. In 2015 ASABE annual international meeting (p. 1). American Society of Agricultural and Biological Engineers.

Crichton, S., L. Shrestha, A. Hurlbert, and B. Sturm. 2018. Use of hyperspectral imaging for the prediction of moisture content and chromaticity of raw and pretreated apple slices during convection drying. *Drying Technology* 36 (7):804–16. doi: 10.1080/07373937.2017.1356847.

Cui, Z.-W., S.-Y. Xu, D.-W. Sun, and W. Chen. 2005. Temperature Changes during Microwave-Vacuum Drying of Sliced Carrots. *Drying Technology* 23 (5):1057–74. doi:10.1081/DRT-200059136.

Cui, Z.-W., S.-Y. Xu, and D.-W. Sun. 2004a. Microwave–vacuum drying kinetics of carrot slices. *Journal of Food Engineering* 65 (2):157–64. doi:10.1016/j.jfoodeng.2004.01.008.

Cui, Z.-W., S.-Y. Xu, and D.-W. Sun. 2004b. Effect of Microwave-Vacuum Drying on the Carotenoids Retention of Carrot Slices and Chlorophyll Retention of Chinese Chive Leaves. *Drying Technology* 22 (3):563–75. doi:10.1081/DRT-120030001.

Cui, Z.-W., S.-Y. Xu, and D.-W. Sun. 2003. Dehydration of Garlic Slices by Combined Microwave-Vacuum and Air Drying. *Drying Technology* 21 (7):1173–84. doi:10.1081/DRT-120023174.

Czaja, T., E. Kuzawińska, A. Sobota, and R. Szostak. 2018. Determining moisture content in pasta by vibrational spectroscopy. *Talanta* 178:294–8. doi: 10.1016/j.talanta.2017.09.050.

Dai, Q., J.-H. Cheng, D.-W. Sun, Z. Zhu, and H. Pu. 2016. Prediction of total volatile basic nitrogen contents using wavelet features from visible/near-infrared hyperspectral images of prawn (Metapenaeus ensis). *Food Chemistry* 197:257–65. doi:10.1016/j.foodchem.2015.10.073.

Delwiche, S. R. 2015. Basics of spectroscopic analysis. In *Hyperspectral imaging technology in food and agriculture* , ed. B. Park, & R. Lu, 9–56. New York, USA: Springer.

Dénes, L., V. Zsom-Muha, L. Baranyai, and J. Felföldi. 2012. Modelling of apple slice moisture content by optical methods. *Acta Alimentaria* 41 (Supplement 1):39–51. doi: 10.1556/AAlim.41.2012.Suppl.4.

Devahastin, S., and C. Niamnuy. 2010. Invited review: Modelling quality changes of fruits and vegetables during drying: A review. *International Journal of Food Science & Technology* 45 (9):1755–67. doi: 10.1111/j.1365-2621.2010.02352.x.

Dufour, É. 2009. Principles of infrared spectroscopy. In *Infrared spectroscopy for food quality analysis and control*, ed. D.-W. Sun, 3–25. San Diego, USA: Academic Press.

Elavarasan, K., B. A. Shamasundar, F. Badii, and N. Howell. 2016. Angiotensin I-converting enzyme (ACE) inhibitory activity and structural properties of oven- and freeze-dried protein hydrolysate from fresh water fish (Cirrhinus mrigala). *Food Chemistry* 206:210–6. doi: 10.1016/j.foodchem.2016.03.047.

Fan, F.,. P. Xiang, and L. Zhao. 2021. Vibrational spectra analysis of amorphous lactose in structural transformation: Water/temperature plasticization, crystal formation, and molecular mobility. *Food Chemistry* 341 (Pt 1):128215. doi: 10.1016/j.foodchem.2020.128215.

Fellows, P. J. 2009. Dehydration. In *Food processing technology*, ed. P. J. Fellows,. 3rd ed., 481–524. Cambridge, UK: Woodhead Publishing.

Feng, Y. Z., and D.-W. Sun. 2012. Application of hyperspectral imaging in food safety inspection and control: A review. *Critical Reviews in Food Science and Nutrition* 52 (11):1039–58. doi: 10.1080/10408398.2011.651542.

Ferreira, D. S., O. F. Galão, J. A. L. Pallone, and R. J. Poppi. 2014. Comparison and application of near-infrared (NIR) and mid-infrared (MIR) spectroscopy for determination of quality parameters in soybean samples. *Food Control.* 35 (1):227–32. doi: 10.1016/j.foodcont.2013.07.010.

Galvis-Sánchez, A. C., I. C. Santos, R. B. R. Mesquita, J. A. Lopes, A. O. S. S. Rangel, and I. Delgadillo. 2013. Application of mid- and near-infrared spectroscopy for the control and chemical evaluation of brine solutions and traditional sea salts. *Food Analytical Methods* 6 (2):470–80. doi: 10.1007/s12161-012-9458-7.

Gonzalez-Mohino, A., T. Perez-Palacios, T. Antequera, J. Ruiz-Carrascal, L. S. Olegario, and S. Grassi. 2020. Monitoring the processing of dry fermented sausages with a portable NIRS device. *Foods* 9 (9):1294. doi: 10.3390/foods9091294.

Gowen, A. A., F. Marini, C. Esquerre, C. O'Donnell, G. Downey, and J. Burger. 2011. Time series hyperspectral chemical imaging data: Challenges, solutions and applications. *Analytica Chimica Acta* 705 (1-2):272–82. doi: 10.1016/j.aca.2011.06.031.

Guo, Q., D.-W. Sun, J. H. Cheng, and Z. Han. 2017. Microwave processing techniques and their recent applications in the food industry. *Trends in Food Science & Technology* 67:236–47. doi: 10.1016/j.tifs.2017.07.007.

Huang, H., H. Yu, H. Xu, and Y. Ying. 2008. Near infrared spectroscopy for on/in-line monitoring of quality in foods and beverages: A review. *Journal of Food Engineering* 87 (3):303–13. doi: 10.1016/j.jfoodeng.2007.12.022.

Huang, H., Y. Shen, Y. Guo, P. Yang, H. Wang, S. Zhan, H. Liu, H. Song, and Y. He. 2017. Characterization of moisture content in dehydrated scallops using spectral images. *Journal of Food Engineering* 205:47–55. doi: 10.1016/j.jfoodeng.2017.02.018.

Huang, M., Q. Wang, M. Zhang, and Q. Zhu. 2014. Prediction of color and moisture content for vegetable soybean during drying using hyperspectral imaging technology. *Journal of Food Engineering* 128: 24–30. doi: 10.1016/j.jfoodeng.2013.12.008.

Huang, M., W. Zhao, Q. Wang, M. Zhang, and Q. Zhu. 2015. Prediction of moisture content uniformity using hyperspectral imaging technology during the drying of maize kernel. *International Agrophysics* 29 (1):39–46. doi: 10.1515/intag-2015-0012.

Ishikawa, D., G. Ueno, and T. Fujii. 2017. Estimation method of moisture content at the meat surface during drying process by NIR pectroscopy and its application for monitoring of water activity. *Japan Journal of Food Engineering* 18 (3):135–43. doi: 10.11301/jsfe.17493.

Kamruzzaman, M., Y. Makino, and S. Oshita. 2016. Parsimonious model development for real-time monitoring of moisture in red meat using hyperspectral imaging. *Food Chemistry* 196:1084–91. doi: 10.1016/j.foodchem.2015.10.051.

Kauppinen, A., M. Toiviainen, O. Korhonen, J. Aaltonen, K. Jarvinen, J. Paaso, M. Juuti, and J. Ketolainen. 2013. In-line multipoint near-infrared spectroscopy for moisture content quantification during freeze-drying. *Analytical Chemistry* 85 (4):2377–84. doi: 10.1021/ac303403p.

Lee, D., S. Lohumi, B. K. Cho, S. H. Lee, and H. Jung. 2020. Determination of derying patterns of radish slabs under different drying methods using hyperspectral imaging coupled with multivariate analysis. *Foods* 9 (4):484. doi: 10.3390/foods9040484.

Lei, T., and D.-W. Sun. 2019. Developments of nondestructive techniques for evaluating quality attributes of cheeses: A review. *Trends in Food Science & Technology* 88:527–42. doi: 10.1016/j.tifs.2019.04.013.

Lei, T., and D.-W. Sun. 2020. A novel NIR spectral calibration method: Sparse coefficients wavelength selection and regression (SCWR). *Analytica Chimica Acta* 1110:169–80. doi: 10.1016/j.aca.2020.03.007.

Lei, T., X. H. Lin, and D.-W. Sun. 2019. Rapid classification of commercial Cheddar cheeses from different brands using PLSDA, LDA and SPA–LDA models built by hyperspectral data. *Journal of Food Measurement and Characterization* 13 (4):3119–29. doi: 10.1007/s11694-019-00234-0.

Li, J., and Z. Q. Qian. 2017. The application of image acquisition and analysis techniques to the field of drying. *Food Engineering Reviews* 9 (1):13–35. doi: 10.1007/s12393-016-9146-2.

Li, J., Z. Li, N. Wang, G. S. V. Raghavan, Y. Pei, C. Song, and G. Zhu. 2020. Novel sensing technologies during the food drying process. *Food Engineering Reviews* 12 (2):121–48. doi: 10.1007/s12393-020-09215-2.

Lin, X., and D.-W. Sun. 2020a. Recent developments in vibrational spectroscopic techniques for tea quality and safety analyses. *Trends in Food Science & Technology* 104:163–76. doi: 10.1016/j.tifs.2020.06.009.

Lin, X., and D.-W. Sun. 2020b. Investigation of moisture distribution of ginger slices and splits during hot-air drying and rehydration procedures by NIR hyperspectral imaging. In Sensing for agriculture and food quality and safety XII, ed. M. S. Kim, B. A. Chin, & B. K. Cho, Vol. 11421, 114210D. Internatonal Society for Optics and Photonics. doi: 10.1117/12.2558213.

Lin, X., J. L. Xu, and D.-W. Sun. 2019. Investigation of moisture content uniformity of microwave-vacuum dried mushroom (Agaricus bisporus) by NIR hyperspectral imaging. *LWT-Food Science and Technology* 109:108–17. doi: 10.1016/j.lwt.2019.03.034.

Lin, X., J. L. Xu, and D.-W. Sun. 2021. Comparison of moisture uniformity between microwave-vacuum and hot-air dried ginger slices using hyperspectral information combined with semivariogram. *Drying Technology* 39 (8):1044–58. doi: 10.1080/07373937.2020.1741006.

Lin, X., J. L. Xu, and D.-W. Sun. 2020. Evaluating drying feature differences between ginger slices and splits during microwave-vacuum drying by hyperspectral imaging technique. *Food Chemistry* 332: 127407. doi: 10.1016/j.foodchem.2020.127407.

Liu, C., W. Liu, X. Lu, W. Chen, J. Yang, and L. Zheng. 2016. Potential of multispectral imaging for real-time determination of colour change and moisture distribution in carrot slices during hot air dehydration. *Food Chemistry* 195:110–6. doi: 10.1016/j.foodchem.2015.04.145.

Liu, D., D.-W. Sun, and X. A. Zeng. 2014. Recent advances in wavelength selection techniques for hyperspectral image processing in the food industry. *Food and Bioprocess Technology* 7 (2):307–23. doi: 10.1007/s11947-013-1193-6.

Liu, W., M. Zhang, B. Bhandari, and D. Yu. 2021. A novel combination of LF-NMR and NIR to intelligent control in pulse-spouted microwave freeze drying of blueberry. *LWT-Food Science and Technology* 137:110455. doi: 10.1016/j.lwt.2020.110455.

Liu, Y., D.-W. Sun, J. H. Cheng, and Z. Han. 2018. Hyperspectral imaging sensing of changes in moisture content and color of beef during microwave heating process. *Food Analytical Methods* 11 (9): 2472–84. doi: 10.1007/s12161-018-1234-x.

Liu, Y., H. Pu, and D.-W. Sun. 2017. Hyperspectral imaging technique for evaluating food quality and safety during various processes: A review of recent applications. *Trends in Food Science & Technology* 69:25–35. doi: 10.1016/j.tifs.2017.08.013.

Liu, Y., Y. Sun, A. Xie, H. Yu, Y. Yin, X. Li, and X. Duan. 2017. Potential of hyperspectral imaging for rapid prediction of anthocyanin content of purple-fleshed sweet potato slices during drying process. *Food Analytical Methods* 10 (12):3836–46. doi: 10.1007/s12161-017-0950-y.

Lohumi, S., S. Lee, H. Lee, and B. K. Cho. 2015. A review of vibrational spectroscopic techniques for the detection of food authenticity and adulteration. *Trends in Food Science & Technology* 46 (1):85–98. doi: 10.1016/j.tifs.2015.08.003.

Lu, R., and B. Park. 2015. Introduction. In *Hyperspectral imaging technology in food and agriculture*, ed. B. Park, & R. Lu, 3–7. New York, USA: Springer.

Lu, R., and Y. R. Chen. 1999. Hyperspectral imaging for safety inspection of food and agricultural products. In *Pathogen detection and remediation for safe eating*, ed. Y. R. Chen, Vol. 3544, 121–33. Bellingham, USA: International Society for Optics and Photonics.

Ma, J., H. Pu, and D.-W. Sun. 2018. Predicting intramuscular fat content variations in boiled pork muscles by hyperspectral imaging using a novel spectral pre-processing technique. *LWT* 94:119–28. doi:10.1016/j.lwt.2018.04.030.

Ma, J, and D.-W. Sun. 2020. Prediction of monounsaturated and polyunsaturated fatty acids of various processed pork meats using improved hyperspectral imaging technique. *Food Chemistry* 321: 126695 doi:10.1016/j.foodchem.2020.126695.

Ma, J., D.-W. Sun, B. Nicolai, H. Pu, P. Verboven, Q. Wei, and Z. Liu. 2019a. Comparison of spectral properties of three hyperspectral imaging (HSI) sensors in evaluating main chemical compositions of cured pork. *Journal of Food Engineering* 261:100–8. doi:10.1016/j.jfoodeng.2019.05.024.

Ma, J., D.-W. Sun, H. B. Pu, J. H. Cheng, and Q. Y. Wei. 2019b. Advanced techniques for hyperspectral imaging in the food industry: Principles and recent applications. *Annual Review of Food Science and Technology* 10:197–220. doi: 10.1146/annurev-food-032818-121155.

Ma, J., D.-W. Sun, and H. Pu. 2016. Spectral absorption index in hyperspectral image analysis for predicting moisture contents in pork longissimus dorsi muscles. *Food Chemistry* 197 (Pt A):848–54. doi: 10.1016/j.foodchem.2015.11.023.

Ma, J., D.-W. Sun, and H. Pu. 2017. Model improvement for predicting moisture content (MC) in pork longissimus dorsi muscles under diverse processing conditions by hyperspectral imaging. *Journal of Food Engineering* 196:65–72. doi: 10.1016/j.jfoodeng.2016.10.016.

Ma, J., D.-W. Sun, J. H. Qu, and H. Pu. 2017. Prediction of textural changes in grass carp fillets as affected by vacuum freeze drying using hyperspectral imaging based on integrated group wavelengths. *Lwt - Food Science and Technology* 82:377–85. doi: 10.1016/j.lwt.2017.04.040.

Ma, J., J. H. Qu, and D.-W. Sun. 2017. Developing hyperspectral prediction model for investigating dehydrating and rehydrating mass changes of vacuum freeze dried grass carp fillets. *Food and Bioproducts Processing* 104:66–76. doi: 10.1016/j.fbp.2017.04.007.

Mohammadi-Moghaddam, T., S. M. A. Razavi, M. Taghizadeh, B. Pradhan, A. Sazgarnia, and A. Shaker-Ardekani. 2018. Hyperspectral imaging as an effective tool for prediction the moisture content and textural characteristics of roasted pistachio kernels. *Journal of Food Measurement and Characterization* 12 (3):1493–502. doi: 10.1007/s11694-018-9764-x.

Moscetti, R., B. Sturm, S. O. Crichton, W. Amjad, and R. Massantini. 2018. Postharvest monitoring of organic potato (cv. Anuschka) during hot-air drying using visible-NIR hyperspectral imaging. *Journal of the Science of Food and Agriculture* 98 (7):2507–17. doi: 10.1002/jsfa.8737.

Moscetti, R., F. Raponi, S. Ferri, A. Colantoni, D. Monarca, and R. Massantini. 2018. Real-time monitoring of organic apple (var. Gala) during hot-air drying using near-infrared spectroscopy. *Journal of Food Engineering* 222:139–50. doi: 10.1016/j.jfoodeng.2017.11.023.

Moscetti, R., R. P. Haff, S. Ferri, F. Raponi, D. Monarca, P. Liang, and R. Massantini. 2017. Real-time monitoring of organic carrot (var. Romance) during hot-air drying using near-infrared spectroscopy. *Food and Bioprocess Technology* 10 (11):2046–59. doi: 10.1007/s11947-017-1975-3.

Netto, J. M. S., F. A. Honorato, P. M. Azoubel, L. E. Kurozawa, and D. F. Barbin. 2021. Evaluation of melon drying using hyperspectral imaging technique in the near infrared region. *LWT-Food Science and Technology* 143:111092. doi: 10.1016/j.lwt.2021.111092.

Nguyen-Do-Trong, N.,. J. C. Dusabumuremyi, and W. Saeys. 2018. Cross-polarized VNIR hyperspectral reflectance imaging for non-destructive quality evaluation of dried banana slices, drying process monitoring and control. *Journal of Food Engineering* 238:85–94. doi: 10.1016/j.jfoodeng.2018.06.013.

Nunes, C. A. 2014. Vibrational spectroscopy and chemometrics to assess authenticity, adulteration and intrinsic quality parameters of edible oils and fats. *Food Research International* 60:255–61. doi: 10.1016/j.foodres.2013.08.041.

Özdoğan, G., X. Lin, and D.-W. Sun. 2021. Rapid and noninvasive sensory analyses of food products by hyperspectral imaging: Recent application developments. *Trends in Food Science & Technology* 111: 151–65. doi:10.1016/j.tifs.2021.02.044.

Pan, Y., D.-W. Sun, J.-H. Cheng, and Z. Han. 2018. Non-destructive Detection and Screening of Non-uniformity in Microwave Sterilization Using Hyperspectral Imaging Analysis. *Food Analytical Methods* 11 (6):1568–80. doi:10.1007/s12161-017-1134-5.

Parasoglou, P.,. E. Parrott, J. Zeitler, J. Rasburn, H. Powell, L. Gladden, and M. Johns. 2010. Quantitative water content measurements in food wafers using terahertz radiation. *Terahertz Science and Technology* 3 (4):176–82.

Pedreschi, F., V. H. Segtnan, and S. H. Knutsen. 2010. On-line monitoring of fat, dry matter and acrylamide contents in potato chips using near infrared interactance and visual reflectance imaging. *Food Chemistry* 121 (2):616–20. doi: 10.1016/j.foodchem.2009.12.075.

Porep, J. U., D. R. Kammerer, and R. Carle. 2015. On-line application of near infrared (NIR) spectroscopy in food production. *Trends in Food Science & Technology* 46 (2):211–30. doi: 10.1016/j.tifs.2015.10.002.

Pu, Y. Y., and D.-W. Sun. 2015. Vis-NIR hyperspectral imaging in visualizing moisture distribution of mango slices during microwave-vacuum drying. *Food Chemistry* 188:271–8. doi: 10.1016/j.foodchem.2015.04.120.

Pu, Y. Y., and D.-W. Sun. 2016. Prediction of moisture content uniformity of microwave-vacuum dried mangoes as affected by different shapes using NIR hyperspectral imaging. *Innovative Food Science & Emerging Technologies* 33:348–56. doi: 10.1016/j.ifset.2015.11.003.

Pu, Y. Y., and D.-W. Sun. 2017. Combined hot-air and microwave-vacuum drying for improving drying uniformity of mango slices based on hyperspectral imaging visualisation of moisture content distribution. *Biosystems Engineering* 156:108–19. doi: 10.1016/j.biosystemseng.2017.01.006.

Pu, Y. Y., M. Zhao, C. O'Donnell, and D.-W. Sun. 2018. Nondestructive quality evaluation of banana slices during microwave vacuum drying using spectral and imaging techniques. *Drying Technology* 36 (13):1542–53. doi: 10.1080/07373937.2017.1415929.

Qin, J., Y. Ying, and L. Xie. 2013. The detection of agricultural products and food using terahertz spectroscopy: A review. *Applied Spectroscopy Reviews* 48 (6):439–57. doi: 10.1080/05704928.2012.745418.

Qu, J. H., D.-W. Sun, J. H. Cheng, and H. Pu. 2017. Mapping moisture contents in grass carp (Ctenopharyngodon idella) slices under different freeze drying periods by Vis-NIR hyperspectral imaging. *LWT-Food Science and Technology* 75:529–36. doi: 10.1016/j.lwt.2016.09.024.

Retz, S., V. E. Porley, G. von Gersdorff, O. Hensel, S. Crichton, and B. Sturm. 2017. Effect of maturation and freezing on quality and drying kinetics of beef. *Drying Technology* 35 (16):2002–14. doi: 10.1080/07373937.2017.1295051.

Rongtong, B., T. Suwonsichon, P. Ritthiruangdej, and S. Kasemsumran. 2018. Determination of water activity, total soluble solids and moisture, sucrose, glucose and fructose contents in osmotically dehydrated papaya using near-infrared spectroscopy. *Agriculture and Natural Resources* 52 (6):557–64. doi: 10.1016/j.anres.2018.11.023.

Sathyanarayana, D. N. (Ed.). 2004. *Vibrational spectroscopy: theory and applications*. New Age International. https://newagepublishers.com/servlet/nagetbiblio?bno=000843

Sebben, J. A., J. da Silveira Espindola, L. Ranzan, N. Fernandes de Moura, L. F. Trierweiler, and J. O. Trierweiler. 2018. Development of a quantitative approach using Raman spectroscopy for carotenoids determination in processed sweet potato. *Food Chemistry* 245: 1224–31. doi: 10.1016/j.foodchem.2017.11.086.

Shi, H., and P. Yu. 2017. Comparison of grating-based near-infrared (NIR) and Fourier transform mid-infrared (ATR-FT/MIR) spectroscopy based on spectral preprocessing and wavelength selection for the determination of crude protein and moisture content in wheat. *Food Control*. 82:57–65. doi: 10.1016/j.foodcont.2017.06.015.

Shrestha, L., R. Moscetti, S. Crichton, O. Hensel, and B. Sturm. 2018. Organic apples (cv. Elstar) quality evaluation during hot-air drying using Vis/NIR hyperspectral imaging. In *IDS 2018. 21st international drying symposium proceedings*, ed C. C. Juan-Andrés, C. P., Gabriela, and M. P., Antonio, 973–80. Valencia, Spain: Editorial Universitat Politècnica de València.

Sinelli, N., E. Casiraghi, S. Barzaghi, A. Brambilla, and G. Giovanelli. 2011. Near infrared (NIR) spectroscopy as a tool for monitoring blueberry osmo–air dehydration process. *Food Research International* 44 (5):1427–33. doi: 10.1016/j.foodres.2011.02.046.

Sirisomboon, P., M. Tanaka, T. Kojima, and P. Williams. 2012. Nondestructive estimation of maturity and textural properties on tomato 'Momotaro' by near infrared spectroscopy. *Journal of Food Engineering* 112 (3):218–26. doi: 10.1016/j.jfoodeng.2012.04.007.

Smith, B. C. 2003. *Quantitative spectroscopy: Theory and practice*. San Diego, USA: Academic Press. doi: 10.1016/B978-0-12-650358-6.X5000-3.

Stawczyk, J., I. Muñoz, C. Collell, and J. Comaposada. 2009. Control system for sausage drying based on on-line NIR $a_w$ determination. *Drying Technology* 27 (12):1338–43. doi: 10.1080/07373930903383620.

Sturm, B., S. Raut, B. Kulig, J. Münsterer, K. Kammhuber, O. Hensel, and S. O. J. Crichton. 2020. In-process investigation of the dynamics in drying behavior and quality development of hops using visual and environmental sensors combined with chemometrics. *Computers and Electronics in Agriculture* 175:105547. doi: 10.1016/j.compag.2020.105547.

Su, W. H., and D.-W. Sun. 2016. Multivariate analysis of hyper/multi-spectra for determining volatile compounds and visualizing cooking degree during low-temperature baking of tubers. *Computers and Electronics in Agriculture* 127:561–71. doi: 10.1016/j.compag.2016.07.007.

Su, W. H., and D.-W. Sun. 2017. Chemical imaging for measuring the time series variations of tuber dry matter and starch concentration. *Computers and Electronics in Agriculture* 140:361–73. doi: 10.1016/j.compag.2017.06.013.

Su, W. H., and D.-W. Sun. 2018. Fourier transform infrared and Raman and hyperspectral imaging techniques for quality determinations of powdery foods: A review. *Comprehensive Reviews in Food Science and Food Safety* 17 (1):104–22. doi: 10.1111/1541-4337.12314.

Su, W. H., S. Bakalis, and D.-W. Sun. 2018. Fourier transform mid-infrared-attenuated total reflectance (FTMIR-ATR) microspectroscopy for determining textural property of microwave baked tuber. *Journal of Food Engineering* 218:1–13. doi: 10.1016/j.jfoodeng.2017.08.016.

Su, W. H., S. Bakalis, and D.-W. Sun. 2019a. Advanced applications of near/mid-infrared (NIR/MIR) imaging spectroscopy for rapid prediction of potato and sweet potato moisture contents. In 2019 ASABE annual international meeting, 1. American Society of Agricultural and Biological Engineers.

Su, W. H., S. Bakalis, and D.-W. Sun. 2019b. Chemometric determination of time series moisture in both potato and sweet potato tubers during hot air and microwave drying using near/mid-infrared (NIR/MIR) hyperspectral techniques. *Drying Technology* 38 (5-6):806–23. doi: 10.1080/07373937.2019.1593192.

Su, W. H., S. Bakalis, and D.-W. Sun. 2019c. Fingerprinting study of tuber ultimate compressive strength at different microwave drying times using mid-infrared imaging spectroscopy. *Drying Technology* 37 (9):1113–30. doi: 10.1080/07373937.2018.1487450.

Sun, J., X. Zhang, X. Qiu, X. Zhu, T. Zhang, J. Yang, X. Zhang, and H. Wang. 2020. Hyperspectral data for predicting moisture content and distribution in scallops during continuous and intermittent drying. *Drying Technology* 36 (7):1–14.

Sun, Y., Y. Liu, H. Yu, A. Xie, X. Li, Y. Yin, and X. Duan. 2017. Non-destructive prediction of moisture content and freezable water content of purple-fleshed sweet potato slices during drying process using hyperspectral imaging technique. *Food Analytical Methods* 10 (5):1535–46. doi: 10.1007/s12161-016-0722-0.

Tian, X. Y., J. H. Aheto, C. X. Dai, Y. Ren, and J. W. Bai. 2021. Monitoring microstructural changes and moisture distribution of dry-cured pork: A combined confocal laser scanning microscopy and hyperspectral imaging study. *Journal of the Science of Food and Agriculture* 101 (7):2727–35. doi: 10.1002/jsfa.10899.

Tian, X. Y., J. H. Aheto, J. W. Bai, C. Dai, Y. Ren, and X. Chang. 2021. Quantitative analysis and visualization of moisture and anthocyanins content in purple sweet potato by Vis–NIR hyperspectral imaging. *Journal of Food Processing and Preservation* 45 (2):e15128. doi: 10.1111/jfpp.15128.

Tunde-Akintunde, T. Y. 2011. Mathematical modeling of sun and solar drying of chilli pepper. *Renewable Energy*. 36 (8):2139–45. doi: 10.1016/j.renene.2011.01.017.

von Gersdorff, G. J. E., B. Kulig, O. Hensel, and B. Sturm. 2021. Method comparison between real-time spectral and laboratory based measurements of moisture content and CIELAB color pattern during dehydration of beef slices. *Journal of Food Engineering* 294:110419. doi: 10.1016/j.jfoodeng.2020.110419.

von Gersdorff, G. J. E., V. E. Porley, S. K. Retz, O. Hensel, S. O. J. Crichton, and B. Sturm. 2018. Drying behavior and quality parameters of dried beef (biltong) subjected to different pre-treatments and maturation stages. *Drying Technology* 36 (1):21–32. doi: 10.1080/07373937.2017.1295979.

Wang, K., D.-W. Sun, and H. Pu. 2017. Emerging non-destructive terahertz spectroscopic imaging technique: Principle and applications in the agri-food industry. *Trends in Food Science & Technology* 67:93–105. doi: 10.1016/j.tifs.2017.06.001.

Wise, B. M., N. B. Gallagher, R. Bro, J. M. Shaver, W. Windig, and R. S. Koch. 2006. PLS Toolbox 3.5 for use with MATLAB. Eigenvector Research Incorporated.

Wokadala, O. C., C. Human, S. Willemse, and N. M. Emmambux. 2020. Rapid non-destructive moisture content monitoring using a handheld portable Vis–NIR spectrophotometer during solar drying of mangoes (Mangifera indica L.). *Journal of Food Measurement and Characterization* 14 (2):790–8. doi: 10.1007/s11694-019-00327-w.

Wu, D., and D.-W. Sun. 2013a. Advanced applications of hyperspectral imaging technology for food quality and safety analysis and assessment: A review — Part I: Fundamentals. *Innovative Food Science & Emerging Technologies* 19:1–14. doi: 10.1016/j.ifset.2013.04.014.

Wu, D., and D.-W. Sun. 2013b. Advanced applications of hyperspectral imaging technology for food quality and safety analysis and assessment: A review — Part II: Applications. *Innovative Food Science & Emerging Technologies* 19:15–28. doi: 10.1016/j.ifset.2013.04.016.

Wu, D., H. Shi, S. Wang, Y. He, Y. Bao, and K. Liu. 2012. Rapid prediction of moisture content of dehydrated prawns using online hyperspectral imaging system. *Analytica Chimica Acta* 726:57–66. doi: 10.1016/j.aca.2012.03.038.

Wu, D., S. Wang, N. Wang, P. Nie, Y. He, D.-W. Sun, and J. Yao. 2012. Application of time series hyperspectral imaging (TS-HSI) for determining water distribution within beef and spectral kinetic analysis during dehydration. *Food and Bioprocess Technology* 6 (11):2943–58. doi: 10.1007/s11947-012-0928-0.

Xie, A., D.-W. Sun, Z. Xu, and Z. Zhu. 2015. Rapid detection of frozen pork quality without thawing by Vis–NIR hyperspectral imaging technique. *Talanta* 139:208–15. doi:10.1016/j.talanta.2015.02.027.

Xie, C. Q., X. L. Li, P. C. Nie, and Y. He. 2013. Application of time series hyperspectral imaging (TS-HSI) for determining water content within tea leaves during drying. *Transactions of the ASABE* 56 (6):1431–40.

Xie, C., X. Li, Y. Shao, and Y. He. 2014. Color measurement of tea leaves at different drying periods using hyperspectral imaging technique. *Plos One* 9 (12):e113422. doi: 10.1371/journal.pone.0113422.

Xu, J. L., A. A. Gowen, and D.-W. Sun. 2018. Time series hyperspectral chemical imaging (HCI) for investigation of spectral variations associated with water and plasticizers in casein based biopolymers.

*Journal of Food Engineering* 218:88–105. doi: 10.1016/j.jfoodeng.2017.09.006.

Yancey, J. W., J. K. Apple, J. F. Meullenet, and J. T. Sawyer. 2010. Consumer responses for tenderness and overall impression can be predicted by visible and near-infrared spectroscopy, Meullenet-Owens razor shear, and Warner-Bratzler shear force. *Meat Science* 85 (3):487–92. doi: 10.1016/j.meatsci.2010.02.020.

Yang, Q., D.-W. Sun, and W. Cheng. 2017. Development of simplified models for nondestructive hyperspectral imaging monitoring of TVB-N contents in cured meat during drying process. *Journal of Food Engineering* 192:53–60. doi: 10.1016/j.jfoodeng.2016.07.015.

Yaseen, T., D.-W. Sun, and J. H. Cheng. 2017. Raman imaging for food quality and safety evaluation: Fundamentals and applications. *Trends in Food Science & Technology* 62:177–89. doi: 10.1016/j.tifs.2017.01.012.

Younas, S., C. Liu, H. Qu, Y. Mao, W. Liu, L. Wei, L. Yan, and L. Zheng. 2020. Multispectral imaging for predicting the water status in mushroom during hot-air dehydration. *Journal of Food Science* 85 (4):903–9. doi: 10.1111/1750-3841.15081.

Younas, S., Y. Mao, C. H. Liu, M. A. Murtaza, Z. Ali, L. Wei, W. Liu, and L. Zheng. 2021. Measurement of water fractions in freeze-dried shiitake mushroom by means of multispectral imaging (MSI) and low-field nuclear magnetic resonance (LF-NMR). *Journal of Food Composition and Analysis* 96:103694. doi: 10.1016/j.jfca.2020.103694.

Younas, S., Y. Mao, C. H. Liu, W. Liu, T. Jin, and L. Zheng. 2021. Efficacy study on the non-destructive determination of water fractions in infrared-dried Lentinus edodes using multispectral imaging. *Journal of Food Engineering* 289:110226. doi: 10.1016/j.jfoodeng.2020.110226.

Yu, P., M. Huang, M. Zhang, and B. Yang. 2019. Optimal wavelength selection for hyperspectral imaging evaluation on vegetable soybean moisture content during drying. *Applied Sciences* 9 (2):331. doi: 10.3390/app9020331.

Zahid, A., Abbas, T. H. Imran, M. A. Qaraqe, K. A. Alomainy, A. Cumming, D. R. S. Abbasi. and Q. H. 2019. Characterization and water content estimation method of living plant leaves using Terahertz waves. *Applied Sciences* 9 (14):2781. doi: 10.3390/app9142781.

Zambrano, M. V., B. Dutta, D. G. Mercer, H. L. MacLean, and M. F. Touchie. 2019. Assessment of moisture content measurement methods of dried food products in small-scale operations in developing countries: A review. *Trends in Food Science & Technology* 88:484–96. doi: 10.1016/j.tifs.2019.04.006.

Zhang, M., H. Chen, A. S. Mujumdar, J. Tang, S. Miao, and Y. Wang. 2017. Recent developments in high-quality drying of vegetables, fruits, and aquatic products. *Critical Reviews in Food Science and Nutrition* 57 (6):1239–55. doi: 10.1080/10408398.2014.979280.

Zheng, J., and L. He. 2014. Surface-enhanced Raman spectroscopy for the chemical analysis of food. *Comprehensive Reviews in Food Science and Food Safety* 13 (3):317–28. doi: 10.1111/1541-4337.12062.